

## NEUROSCIENCE

## A cynomolgus monkey with naturally occurring Parkinson's disease

Hao Li <sup>1,†</sup>, Ling-Yan Su<sup>1,†</sup>, Lixin Yang<sup>2,11,†</sup>, Min Li<sup>2,†</sup>, Qianjin Liu<sup>1,3,†</sup>, Zhenhui Li<sup>1,3,†</sup>, Yan Hu<sup>2,3</sup>, Hongwei Li<sup>1</sup>, Shihao Wu<sup>1,5</sup>, Wenchao Wang<sup>1</sup>, Yingzhou Hu<sup>1</sup>, Zhengbo Wang<sup>1</sup>, Joshua D. Rizak<sup>1</sup>, Baihui Huang<sup>1</sup>, Min Xu<sup>1,3</sup>, Jing Wu<sup>1</sup>, Long-Bao Lv<sup>6</sup>, Christoph W. Turck<sup>1,7,\*</sup>, Yong Yin<sup>8,\*</sup>, Yong-Gang Yao <sup>1,3,4,6,9,\*</sup>, Bing Su<sup>2,6,10,\*</sup> and Xintian Hu <sup>1,4,6,\*</sup>

Evidence for the existence of monkeys with spontaneous Parkinson's disease (PD) has been lacking. Here, we screened macaque colonies at the Kunming Primate Research Center (Association for Assessment and Accreditation of Laboratory Animal Care (AAALAC) accredited), Kunming Institute of Zoology, Chinese Academy of Sciences, which has a large population of monkeys (>2400), to identify naturally occurring PD monkeys. Sixty cynomolgus macaques and rhesus macaques with no experimental experience, housed in single cages of the Kunming Primate Research Center, were selected as the subjects of a preliminary screen procedure to search for naturally occurring PD (Supplementary Fig. S1). The subjects' age, gender and species information are listed in Supplementary Table S1.

Among the 60 monkeys, a 10-year-old male cynomolgus monkey (ID: #06103) showed severe PD symptoms. It had an overall PD score of over 15 (Fig. 1A), which was evaluated by part A of the improved version of the *Kurlan* scale [1]. The scale has been widely used in old world monkey PD symptoms quantification and its maximum score of part A is 20. The details of the rating scale are provided in Supplementary Table S2. According to UK Parkinson's Disease Society Brain Bank clinical diagnostic criteria [2], the core clinical symptoms used in PD diagnosis are bradykinesia, which is the essential criterion,

and at least one of two other symptoms, namely tremor and/or postural instability. A closer examination of the seven individual behavioral items' scores that make up part A of the improved *Kurlan* scale showed that they were all above zero (Fig. 1B). Among them, there were all the behavioral symptoms employed in human PD diagnosis, including bradykinesia, tremor and postural instability, which was reflected in the balance, gait and gross motor skill disability of the monkey. Thus, we concluded that the cynomolgus monkey (ID: #06103) displayed all the testable diagnostic PD symptoms (Fig. 1A and B; Supplementary Video S1), completely fulfilled the clinical PD diagnostic criteria, and therefore was qualified as a monkey with Parkinsonism.

Following the classic PD symptoms assessments described above, a pharmacological validation was carried out. Compared with the symptom validation, which is a relatively rough quantification of the animal's daily behavior, a pharmacological validation is a better controlled and more PD specific quantitative test. In this test, the treatment of the monkey with a classic PD drug levodopa (L-dopa) resulted in positive responses with a significant total PD score reduction from 17.7 to 9.3 ( $P = 0.022$ , Fig. 1C; Supplementary Video S2). All seven individual items' scores were reduced, with six out of seven being significant (Fig. 1D). Together, the above data

revealed very effective treatment responses and provided strong evidence for the pharmacological validation.

To confirm the L-dopa treatment effects, apomorphine (Apo), another classic PD drug which is an agonist of dopamine D1 receptor [2], was used. The monkey again displayed a positive treatment response with the total PD score significantly reduced from 15.3 to 10.3 ( $P = 0.023$ , Fig. 1E; Supplementary Video S3). The scores of three out of the seven items showed a significant reduction, another three showed a trend of reduction and one, gross motor skill, remained unchanged (Fig. 1F), also revealing effective treatment responses and providing a clear pharmacological validation. The same pharmacological tests were carried out on three control monkeys, which had an average total PD score 0.67 (the PD score range of normal monkeys is 0–4). All control animals showed no response to both PD drug treatments (Supplementary Fig. S2). Taken together, both the symptom assessment and pharmacological tests strongly suggested that we had successfully identified a monkey with Parkinsonism.

The key pathology hallmark of PD is severe loss of dopaminergic neurons and obvious morphological changes of the surviving dopaminergic neurons in the substantia nigra pars compacta (SNpc) [2,3]. Tyrosine hydroxylase (TH) immunostaining, which is a classic staining method for visualization of dopaminergic

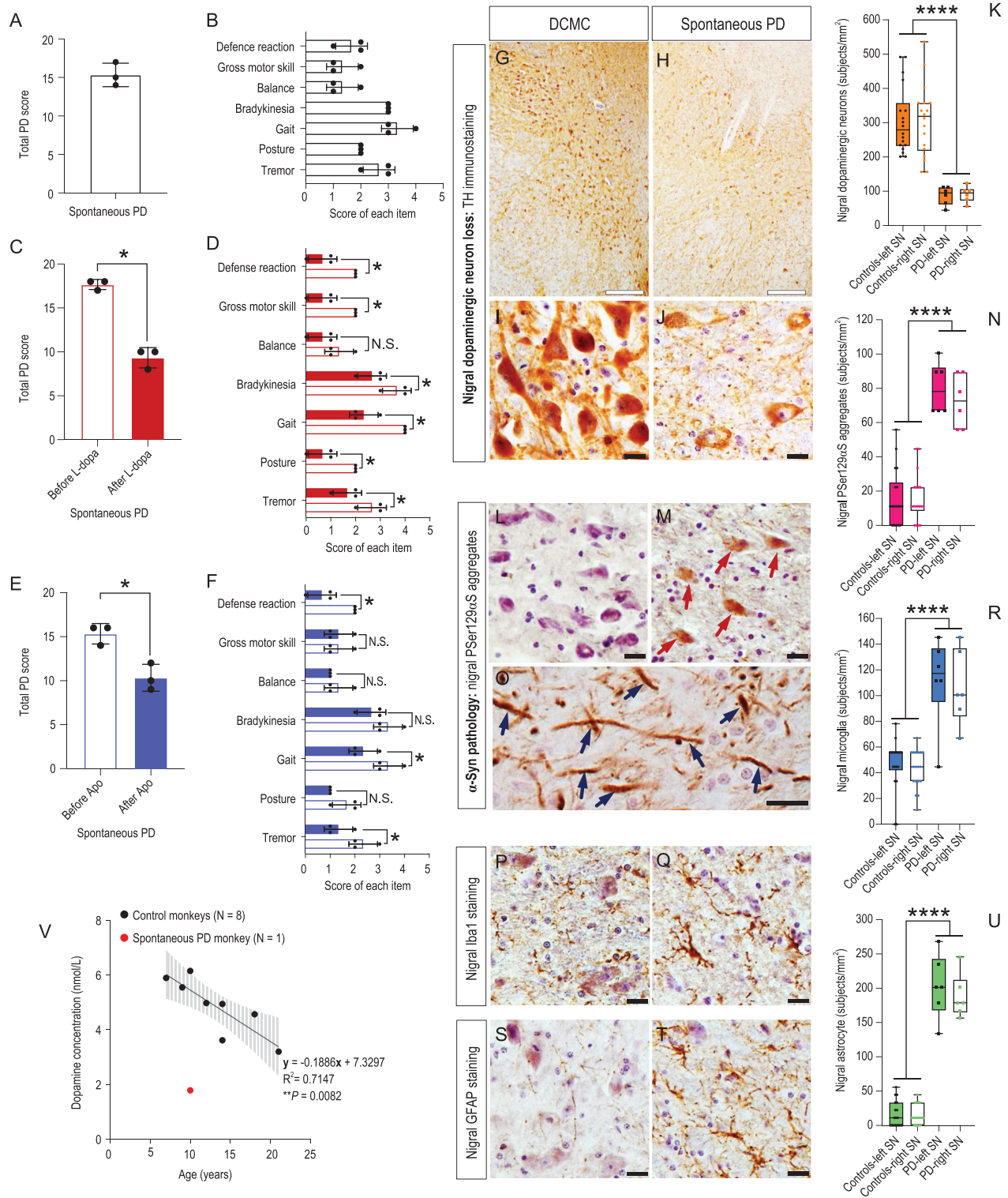


**Figure 1.** Classic Parkinsonian symptoms and pathologic hallmarks of the spontaneous PD monkey (#06103). (A) Quantified by the improved *Kurlan* scale, the monkey had a total PD score above 15 out of a maximum of 20, demonstrating severe PD symptoms. (B) The seven items' scores that constitute the improved *Kurlan* scale were all above zero, revealing the monkey had all the diagnostic PD symptoms. The total PD score was the sum of the seven individual item scores. (C) The total PD score of the monkey was reduced significantly from 17.7 to 9.3 after a classic PD drug L-dopa treatment, indicating a significant positive response to the treatment. (D) The scores of the seven individual items were all reduced after the L-dopa treatment, and the reduction of six items out of the seven were significant. Both C and D provide strong evidence for pharmacological validation. (E) The total PD score of the monkey was reduced significantly from 15.3 to 10.3 after the apomorphine (Apo, an agonist of dopamine D1 receptor)

**Figure 1.** Continued. treatment, indicating a significant improvement of PD symptoms by dopamine D1 receptor activation. (F) The scores of the seven individual items were all reduced after Apo treatment except for gross motor skill, and three out of the seven items were significant. These data further confirmed the above results from the L-dopa treatment. The data were quantified from three video clips of each experimental condition and presented as mean  $\pm$  SD. Non-parametric statistics (Mann-Whitney test) were used (\*,  $P < 0.05$ ). (G and H) Under lower resolution images (4 $\times$ ), nigral TH immunostaining of the death-condition-matched control (DCMC, #071809) and spontaneous PD monkey indicated the overall nigral dopaminergic neuron loss of the spontaneous PD monkey: fewer nigral dopaminergic neurons that were lightly stained survived in the spontaneous PD monkey compared with the DCMC. (I and J) Under higher resolution images (40 $\times$ ), nigral TH immunostaining of the spontaneous PD monkey showed obviously less dopaminergic neurons with weakly stained somata and fewer neurites compared with that of the DCMC. (K) Quantitative analysis demonstrated that the nigral dopaminergic neuron number of the spontaneous PD monkey was about 70% less compared with that of the controls (\*\*\*\*,  $P < 0.001$ ). (L and M) P $\text{Ser129}\alpha\text{S}$  immunostaining of the SNs revealed that there were more P $\text{Ser129}\alpha\text{S}$  aggregates (red arrows) in the spontaneous PD monkey compared with the DCMC. (N) The number of P $\text{Ser129}\alpha\text{S}$  aggregates in the spontaneous PD monkey's SN was five times higher (\*\*\*\*,  $P < 0.001$ ). (O) P $\text{Ser129}\alpha\text{S}$  aggregates in the nigral neuron's processes were found in the spontaneous PD monkey (blue arrows). (P and Q) Iba1 immunostaining of the monkeys' SNs revealed that there were more activated microglia in the spontaneous PD monkey compared with the DCMC. (R) The number of activated microglia in the spontaneous PD monkey's SN was 2.5 times larger than the controls (\*\*\*\*,  $P < 0.001$ ). (S and T) GFAP immunostaining in the monkeys' SNs revealed that there were more activated astrocytes in the spontaneous PD monkey compared with the DCMC. (U) The number of the activated astrocyte in the spontaneous PD monkey's SN was 12.5 times larger than the controls (\*\*\*\*,  $P < 0.001$ ). Scale bars: hollow black: 200  $\mu\text{m}$ ; solid black: 20  $\mu\text{m}$ . Data in K, N, R and U are median with minimum to maximum. Non-parametric statistics (Mann-Whitney test) was used. (V) Lower cerebrospinal fluid (CSF) dopamine level of the spontaneous PD monkey compared to the eight normal controls. The dopamine level was measured by a high-pressure liquid chromatography. Black dots represent dopamine concentrations of the eight normal control monkeys. The black line is the regression curve, and the gray shadow represents the 95% confidence interval of the control monkeys' CSF dopamine concentration. The red dot represents the CSF dopamine concentration of the spontaneous PD monkey, which is located way outside the 95% confidence interval. \*,  $P < 0.05$ ; \*\*,  $P < 0.01$  and \*\*\*\*,  $P < 0.001$ .

neurons, clearly showed that much fewer dopaminergic neurons were stained in the monkey with Parkinsonism compared with those in the death-condition-matched control (DCMC, ID: #071809) under lower resolution images (Fig. 1G and H). Under higher resolution images, obvious morphological changes of the surviving dopaminergic neurons, such as weaker-stained somata and fewer neurites could be observed (Fig. 1I and J). A quantitative analysis demonstrated an approximate 70% loss of dopaminergic neurons (Fig. 1K) in the SNpc of the monkey with Parkinsonism compared with the controls (the DCMC plus two age-matched controls; Supplementary Data). Collectively, the monkey with spontaneous Parkinsonism clearly possessed the most important PD pathology hallmark: severe loss of nigral dopaminergic neurons and obvious morphological changes.

Another important PD hallmark, Lewy body (LB) pathology, which appears in 77% to 95% PD patients according to different studies [3,4], is commonly illustrated by phosphorylated-serine129  $\alpha$ -synuclein (P $\text{Ser129}\alpha\text{S}$ ) immunostaining. Although classical Lewy bodies were not identified in this monkey, the  $\alpha$ -synuclein pathology, which is also termed P $\text{Ser129}\alpha\text{S}$  aggregates, was revealed by this staining. The

$\alpha$ -synuclein pathology is considered as an early stage of the Lewy pathology based on the following reasons: (i) aggregated  $\alpha$ -synuclein is the major component of Lewy bodies and Lewy neurites [5], and about 90% of the  $\alpha$ -synuclein aggregates consist of P $\text{Ser129}\alpha\text{S}$  [6]; (ii) the LB formation is probably triggered by abnormal accumulation of P $\text{Ser129}\alpha\text{S}$  in the cytoplasm [3,7]. Illustrated by staining with antibody *ab59264*, one of the most commonly used antibodies for P $\text{Ser129}\alpha\text{S}$  immunostaining [7], a greater number of P $\text{Ser129}\alpha\text{S}$  aggregates in the cytoplasm were found in the SNpc of the monkey with Parkinsonism compared with the DCMC (Fig. 1L and M). A quantitative analysis revealed that the number of P $\text{Ser129}\alpha\text{S}$  aggregates was 5 times greater in the monkey with Parkinsonism than those in the controls (Fig. 1N). Moreover, some spindle-like or thread-like P $\text{Ser129}\alpha\text{S}$  aggregates were also identified in the nigral neuron processes of the monkey with Parkinsonism; more evidence of the  $\alpha$ -synuclein pathology (Fig. 1O). To further verify the specificity of the immunostaining results, a more specific monoclonal antibody (*ab51253*) was used to label the P $\text{Ser129}\alpha\text{S}$  in the locus ceruleus (LC) of the monkey with Parkinsonism, which resulted in similar staining results (Supplementary Fig. S3). In summary, the

immunostaining results clearly illustrated that the PD candidate monkey had the  $\alpha$ -synuclein pathologic changes, which is considered an early stage of the Lewy pathology.

A less emphasized but equally important pathology hallmark is the gliosis reported in PD patients [8]. It includes an increased number of microglia cells with enlarged somata and reduced but thickened neurites, and an increased number of astrocytes with expressed glial fibrillary acidic protein (GFAP). To explore the glia activation in the SN region of the monkey with Parkinsonism, Iba1 and GFAP antibodies were used to label the microglia and astrocytes, respectively. A large number of activated microglia (Fig. 1P and Q) revealed by enlarged somata (Supplementary Fig. S4) and astrocytes containing GFAP (Fig. 1S and T) were identified in SNpc of the monkey with Parkinsonism. Quantitative analyses showed a significant 2.5-fold increase of microglia (Fig. 1R) and a 12.5-fold increase of astrocyte numbers (Fig. 1U) in this monkey. Moreover, consistent with what is observed in PD patients [9], a significantly lower cerebrospinal fluid (CSF) dopamine level was identified in the monkey with Parkinsonism (Fig. 1V, red dot). Taken together, the identified monkey (ID: #06103) displayed all the classic PD

pathology hallmarks, and therefore was fully qualified as a spontaneous PD monkey in terms of pathological changes, in addition to the behavioral and pharmacological validations.

This PD monkey was 10 years old, which corresponds to a human age of around 30–40 [10]. Since most early-onset PD patients have genetic contributions [2], we carried out a sequencing analysis of 11 known PD risk genes and delineated four missense mutations in *LRRK2* and *ATP13A2* in this monkey (Supplementary Figs S5 and 6). Follow up functional studies suggested that the *LRRK2* mutations were likely causal for PD pathology (Supplementary Figs S7 and 8).

Collectively, four lines of evidence, including typical PD clinical symptoms, pharmacological responses, pathology hallmarks and genetic mutations, strongly suggested that we had identified a cynomolgus monkey with spontaneous PD. This indicates that PD is not a uniquely human disease and, therefore, as close relatives to humans, monkeys are ideal candidates to develop genuine ‘animal versions of PD’, in which the etiology and pathogenesis are evolutionally conserved. Furthermore, it allows one to compare similarities and differences of PD development between species and to understand PD pathogenesis from an evolutionary point of view.

## SUPPLEMENTARY DATA

Supplementary data are available at [NSR](#) online.

## ACKNOWLEDGEMENTS

We would like to thank Prof. Min He from Kunming Medical University for her professional review of all the pathologic data, Limin Wang and Yihua Liu for their hard work, and Ling Zhao and Zhengfei Hu for their animal care. We would like to thank Dr. Nanhui Chen for his help in MRI scanning.

## FUNDING

This work was supported by the Key-Area Research and Development Program of Guangdong Province (2019B030335001), the National Key R&D Program of China (2018YFA0801403), the Strategic Priority Research Program of the Chinese Academy of Sciences (CAS) (XDB32060200 and XDB32020200), the National Program for Key Basic Research Projects (2015CB755605), the National Natural Science Foundation of China (81941014, 81471312, 81771387, 81460352, 81500983, 31700897, 31700910, 31800901, 31960178, 91732302), the Applied Basic Research Programs of Science and Technology Commission Foundation of Yunnan Province (2017FB109, 2018FB052, 2018FB053, 2019FA007, 202001AT070130), the China Postdoctoral Science Foundation (2018M631105) and CAS ‘Light of West China’ Program.

**Conflict of interest statement.** None declared.

Hao Li <sup>1,†</sup>, Ling-Yan Su<sup>1,†</sup>, Lixin Yang<sup>2,11,†</sup>, Min Li<sup>2,†</sup>, Qianjin Liu<sup>1,3,†</sup>, Zhenhui Li<sup>1,3,†</sup>, Yan Hu<sup>2,3</sup>, Hongwei Li<sup>1</sup>, Shihao Wu<sup>1,5</sup>, Wenchao Wang<sup>1</sup>, Yingzhou Hu<sup>1</sup>, Zhengbo Wang<sup>1</sup>, Joshua D. Rizak<sup>1</sup>, Baihui Huang<sup>1</sup>, Min Xu<sup>1,3</sup>, Jing Wu<sup>1</sup>, Long-Bao Lv<sup>6</sup>, Christoph W. Turck<sup>1,7,\*</sup>, Yong Yin<sup>8,\*</sup>, Yong-Gang Yao <sup>1,3,4,6,9,\*</sup>, Bing Su<sup>2,6,10,\*</sup> and Xintian Hu <sup>1,4,6,\*</sup>

<sup>1</sup>Key Laboratory of Animal Models and Human Disease Mechanisms of the Chinese Academy of Sciences & Yunnan Province, Kunming Institute of Zoology, Chinese Academy of Sciences, China; <sup>2</sup>State Key Laboratory of Genetic Resources and Evolution, Kunming Institute of Zoology, Chinese Academy of Sciences, China; <sup>3</sup>Kunming College of Life Science, University of Chinese Academy of Sciences, China; <sup>4</sup>Center for Excellence in Brain Science and Intelligence Technology, Chinese Academy of Sciences, China; <sup>5</sup>Institute of Neuroscience, CAS Key Laboratory of Primate Neurobiology, State Key Laboratory of Neuroscience, Chinese Academy of Sciences, China; <sup>6</sup>National Resource Center for Non-Human Primates, Kunming Primate Research Center, and National Research Facility for Phenotypic & Genetic Analysis of Model Animals (Primate Facility), Kunming Institute of

Zoology, Chinese Academy of Sciences, China; <sup>7</sup>Max Planck Institute of Psychiatry, Department of Translational Research in Psychiatry, Germany; <sup>8</sup>Department of Rehabilitation Medicine, the Second People’s Hospital of Yunnan Province, China; <sup>9</sup>KIZ – CUHK Joint Laboratory of Bioresources and Molecular Research in Common Diseases, Kunming Institute of Zoology, Chinese Academy of Sciences, China; <sup>10</sup>Center for Excellence in Animal Evolution and Genetics, Chinese Academy of Sciences, China and <sup>11</sup>Shenzhen Key Laboratory for Molecular Biology of Neural Development, Guangdong Provincial Key Laboratory of Brain Connectome and Behavior, CAS Key Laboratory of Brain Connectome and Manipulation, The Brain Cognition and Brain Disease Institute, Shenzhen Institutes of Advanced Technology, Chinese Academy of Sciences, China; Shenzhen-Hong Kong Institute of Brain Science, China

**\*Corresponding authors.** E-mails:

[turck@psych.mpg.de](mailto:turck@psych.mpg.de); [yinyong@ynshhy.com](mailto:yinyong@ynshhy.com); [yaoyg@mail.kiz.ac.cn](mailto:yaoyg@mail.kiz.ac.cn); [sub@mail.kiz.ac.cn](mailto:sub@mail.kiz.ac.cn); [xthu@mail.kiz.ac.cn](mailto:xthu@mail.kiz.ac.cn)

<sup>†</sup>Equally contributed to this work.

## REFERENCES

- Smith RD, Zhang Z and Kurlan R *et al.* *Neuroscience* 1993; **52**: 7–16.
- Kalia LV and Lang AE. *Lancet* 2015; **386**: 896–912.
- Dickson DW. *Parkinsonism Relat Disord* 2018; **46 Suppl 1**: S30–S33.
- Gibb WR. *Neuropathol Appl Neurobiol* 1986; **12**: 223–34.
- Spillantini MG, Schmidt ML and Lee VM *et al.* *Nature* 1997; **388**: 839–40.
- Fujiwara H, Hasegawa M and Dohmae N *et al.* *Nat Cell Biol* 2002; **4**: 160–4.
- Shahmoradian SH, Lewis AJ and Genoud C *et al.* *Nat Neurosci* 2019; **22**: 1099–109.
- Hickman S, Izzy S and Sen P *et al.* *Nat Neurosci* 2018; **21**: 1359–69.
- Jimenez-Jimenez FJ, Alonso-Navarro H and Garcia-Martin E *et al.* *Front Cell Neurosci* 2014; **8**: 369.
- Roth GS, Mattison JA and Ottinger MA *et al.* *Science* 2004; **305**: 1423–6.

# Supplementary Data

## A cynomolgus monkey with naturally occurring Parkinson's disease

Hao Li, Ling-Yan Su, Lixin Yang, Min Li, Qianjin Liu, Zhenhui Li, Yan Hu, Hongwei Li, Shihao Wu, Wenchao Wang, Yingzhou Hu, Zhengbo Wang, Joshua D. Rizak, Baihui Huang, Min Xu, Jing Wu, Long-Bao Lv, Christoph W. Turck\*, Yong Yin\*, Yong-Gang Yao\*, Bing Su\*, and Xintian Hu\*

**\*Corresponding authors (Emails):**

[turck@psych.mpg.de](mailto:turck@psych.mpg.de);

[yinyong@ynshhyy.com](mailto:yinyong@ynshhyy.com);

[yaoyg@mail.kiz.ac.cn](mailto:yaoyg@mail.kiz.ac.cn);

[sub@mail.kiz.ac.cn](mailto:sub@mail.kiz.ac.cn);

[xthu@mail.kiz.ac.cn](mailto:xthu@mail.kiz.ac.cn).

### **This PDF document contains:**

Supplementary Methods

Supplementary Results

Supplementary Figures S1-S10

Supplementary Tables S1-S4

Supplementary References 1-56

## Supplementary Methods

### *Animals and ethics*

The experimental protocols and animal welfare were approved by the Ethics Committee of Kunming Primate Research Center (AAALAC accredited), Kunming Institute of Zoology, Chinese Academy of Sciences. All animals involved in this study were treated also in accordance with the National Institute of Health (U.S.A.) Guide for the Care and Use of Laboratory Animals [8th edition. Washington (DC): National Academies Press; 2011] and the ARRIVE guidelines for reporting animal research [1]. Here, 34 rhesus monkeys (*M. mulatta*) and 26 cynomolgus monkeys (*M. fascicularis*) were selected as the primary subjects for this project based on the following terms, 1) age: 7-30 years old; 2) general status: healthy and without any prior experimental experience. The detailed information of these 60 monkeys is listed in Table S1, and best efforts were made to minimize the suffering of the monkeys involved in this study.

### *Selection and validation procedures for the PD monkey candidates*

The first criterion for selection was the appearance of one or more Parkinsonian symptoms, including bradykinesia, tremor, and postural instability. After the first screen, a 10-year old male cynomolgus monkey (ID: #06103) was identified as a candidate. Next, four quantitative assessments were carried out to validate the monkey was indeed a PD case.

**1) PD behavioral symptoms validation:** PD symptoms of the candidate monkey and three control monkeys were quantified by the well-established *Kurlan* scale (improved version) [2], a widely used scale to quantify PD symptoms in old world monkeys [3].

**2) Pharmacological validation:** the PD monkey candidate and three control monkeys were treated with levodopa (L-dopa) and apomorphine (Apo) to evaluate their responses to the classic PD drugs used clinically for PD patients. Improved responses resemble those observed in PD patients are in support of the monkey suffering from PD.

**3) Pathologic validation:** the pathology hallmarks of PD include severe nigral dopaminergic neuron loss,  $\alpha$ -synuclein pathology, glial cell activation and low dopamine concentration in the brain. This included nigral tyrosine hydroxylase (TH) immunostaining to illustrate dopaminergic neurons, phosphorylated Ser129  $\alpha$ -synuclein immunostaining to illustrate  $\alpha$ -synuclein pathology, and Iba1 and

GFAP immunostaining to show microglia and astrocyte activation, respectively. The dopamine concentration in the cerebrospinal fluid (CSF) of the PD candidate monkey was measured by a high-performance liquid chromatography (HPLC) and then compared with those of eight normal controls.

**4) Genetic analysis and the related functional assays:** to identify PD-related mutations, a total of eleven reported PD risk / causal genes were sequenced for the PD candidate monkey and compared with our genetic database of 1,585 normal cynomolgus monkeys. Afterwards, the functional consequences of the identified mutation(s) were investigated at the cellular level, and RNA-seq was performed to reconstruct the differentially expressed genes and affected pathways.

### ***Detailed information of the four validations***

#### ***1) PD symptoms validation***

To identify and quantify the Parkinsonian symptoms of the PD monkey candidate (ID: #06103), its behavior was video recorded according to a protocol adopted from previous studies [2, 4, 5]. Free moving behavior of the monkey in a single cage was recorded without external disturbance for 1 hour by a digital camera (Sony HDR-XR260, Japan) located 1 meter in front of the cage from 15:00 pm to 16:00 pm. After the recording, the 1-hour video was divided into 3 episodes of 20 minutes each by the experimenter, creating 3 video clips for further behavioral assessment.

The video analysis protocol was adopted from previous studies as well [2, 4, 5]. Two experienced observers were involved in the analysis. The 3 video clips were randomly labeled by the experimenter with numbers from 1 to 3. Blind to the conditions of the monkey, the two observers were assigned the video clips to score independently using the well-established *Kurlan* scale (improved version) [2], which has been widely accepted as a standard scale for PD research on old world monkeys [3].

There are 4 parts in the improved *Kurlan* scale: part A: Parkinsonian features; part B: drug-related side effects; part C: overall level of activity; part D: clinical staging. Only parts A and D were used in this study. The symptom of the PD monkey was marked by part A of this scale [2], which included seven items: tremor, posture, gait, bradykinesia, balance, gross motor skill, and defense reaction. Each item score was evaluated and assigned by the severity of the symptom (*Tremor: 0~3; Posture: 0~2; Gait: 0~4; Bradykinesia: 0~4; Balance: 0~2; Gross motor skill: 0~3; Defense reaction: 0~2*),

and the total PD score was the sum of the scores of the seven items. The total score maximum is 20, and the range of the normal score is about 0-4. For more details, please refer to Table S2. If there was no obvious scoring difference (less than two points) between the two observers, the data was combined to create figures and perform statistics analysis.

The PD monkey candidate's clinical stage, as assessed by part D of the scale, was determined as the most severe stage V according to following three criteria: **1)** bilateral Parkinsonism, obvious by no rotational behavior following apomorphine (Apo) treatment. Usually, monkeys will show obvious rotational behavior after Apo administration if they are hemi-Parkinsonism [4, 6]. Moreover, there were similar severe dopaminergic neuron losses in both the left and right SNs ( $P = 0.801$ ,  $t$ -test); **2)** required assistance to maintain adequate nutrition, which was obvious by difficulties that the monkey had during eating (data not shown); **3)** frequent face-down posture (please refer to Supplementary Videos 1-3).

### **2) Pharmacological validation**

Levodopa (L-dopa) and apomorphine (Apo) are two classic PD treatment drugs and also standard agents in PD animal models' pharmacological validation [7, 8]. The L-dopa treatment effect was evaluated by comparing the monkey's PD score marked by the improved *Kurlan* scale mentioned above before and after the L-dopa administration. Briefly, behavior of the PD monkey candidate was recorded for 1 hour from 15:00 pm to 16:00 pm, and then the PD monkey candidate was intramuscularly injected (*i.m.*) with 2 mL L-dopa (30 mg/kg, V-900425-100MG, Sigma, U.S.A.). After 15 minutes, the behavior of the PD monkey candidate was recorded again for 1 hour from 16:20 pm to 17:20 pm. Drug effects of L-dopa wash out usually takes 9 hours.

Next day, the Apo treatment effect was evaluated in the same way as the L-dopa treatment, except that the dosage was 1 mg/mL, 2 mL, *i.m.* (A4393-100MG, Sigma, U.S.A.).

After these tests, 4 videos of 1 hour each were obtained from the PD monkey candidate. Each individual video was divided into 3 episodes of 20 minutes by the experimenter, creating 12 video clips of 20 minutes each, which were randomly labeled by the experimenter with the numbers from 1 to 12. Conditions of the clips were blind to the two observers who analyzed the videos in the same way as the PD symptoms validation.

### **3) Pathologic validation**

### ***a) Control monkeys' information and brain tissue treatment***

The PD monkey candidate was weak and thin when we first noticed it. It was carefully cared for by veterinarians after that. Not long after the behavioral tests were finished, the monkey died during an unexpected cold night. The body was examined next morning and, thus, the postmortem interval was less than 12 hours. No obvious abnormality was observed during the autopsy, leading us to conclude that the death was probably due to hypothermia.

To verify the pathology hallmarks of the PD monkey candidate, valid controls were needed. There were two kinds of controls in this study. The first was a death-condition-matched control (DCMC), since the brain tissue of the PD monkey candidate was acquired after its sudden death without perfusion. To exclude potential pathology changes that might be caused by the non-perfusion process, brain tissue from an age-matched male cynomolgus monkey (ID: #071809), who also died of cold weather, was acquired within 12 hours without perfusion just like the PD monkey candidate, and was used as a DCMC for PD pathology study. The brain tissues of the two monkeys were all fixed in 4% paraformaldehyde-0.01 M PBS for two weeks, and then they were dehydrated in 20% and 30% sucrose solutions.

The second kind of control was age-matched normal monkeys. To increase the statistic power, two more age-matched monkeys (ID: #071725, and #05103) were first intramuscularly administrated with ketamine (10 mg/kg, 0.05 g/mL, *i.m.*, Zhongmu, Taizhou, China) and then euthanized with pentobarbital sodium (40 mg/mL, 20 mg/kg, *i.m.* Fluka, Germany) for perfusion. After the perfusion, their brains were processed in the same way as the two monkeys of sudden death mentioned above.

### ***b) Determination of the anterior-posterior length (AP length) of the substantia nigra (SN) in monkey brain***

The most important brain area involved in PD pathology is the substantia nigra (SN), a paired flat shaped structure located deeply in the narrow mesencephalon [4, 9]. It is necessary to determine the anterior-posterior length (AP length) of the SN before the sectioning. The length of cynomolgus monkey's SN was determined by referring to "*The Rhesus Monkey Brain in Stereotaxic Coordinates, George Praxinos et al., Academic Press, 1999*" and then verified by a set of MRI scanning data of cynomolgus monkeys from a 3T MRI facility (United Imaging, Shanghai, China) in Kunming Institute of Zoology, Chinese Academy of Sciences.

First, according to the monkey brain atlas, the SN of macaque monkey brain is located at -9.90 mm to -17.78 mm AP from the bregma. As a result, its AP length is 7.88 mm ( $17.78 - 9.90 = 7.88$  mm). Second, using the MRI data, the AP length of the cynomolgus monkeys' SNs was measured with a range from 6.7-7.8 mm. To ensure inclusion of the monkey's whole SN, the total AP length of the cynomolgus monkey's SN was determined as 8.0 mm.

#### ***c) Cutting brain sections for immunostaining***

The total AP length of the monkey's SN was determined as 8.0 mm by the procedure mentioned above. After this, the SN was cut into coronal sections with a thickness of 20  $\mu$ m. The interval between every two sections was 60  $\mu$ m, and, as a result, about 100 sections were obtained from each monkey's SN. All the monkeys' SNs were cut in the same way by a freezing microtome (Leica, CM1850UV-1-1, Germany) at -24 °C.

Next, we needed to pick out the optimum sections of the cut SN for immunostaining. The anatomical criteria for selecting the optimal portion of SN for pathological study was established by Chu *et al.* [10-12], Gundersen *et al.* [13] and also by Dickson *et al.* [9]. The criteria are to select the portion of the SN that overlaps with the third cranial nerve (3n) rootlets. The SN is in the ventral midbrain and defined ventrally by the cerebral peduncle and medially by the 3n rootlets in a coronal section [9, 11]. According to the monkey's atlas, the total AP length of the SN that overlaps with the 3n rootlets is 2.25 mm (-10.80 mm to -13.05 mm AP from bregma), near 30% of the whole SN ( $2.25/8 = 28.13\%$ ), and, according to the criteria, the optimum sections of a SN for staining were around 30 coronal sections, ranging from the 11<sup>th</sup> section to the 40<sup>th</sup> section out of the 100 sections (Fig. S9). As for the three controls, their SNs were sectioned and selected in the same way.

#### ***d) Staining***

The 30 optimum sections of SN were divided into 5 sets for TH, P $\text{Ser}129\alpha\text{S}$ , Iba1, GFAP immunostaining, and hematoxylin & eosin (H & E) staining, respectively. A total of six sections were picked out from every 5 sections among the 30 to form a set for the staining (Fig. S9).

For TH staining, a standard protocol was used [5, 11]: the sections were treated with 3%  $\text{H}_2\text{O}_2$  (5 min, Maixin, Fuzhou, China), 3% triton X-100 (4 min, Solarbio, Beijing, China), 10% goat serum (15 min, Maixin, Fuzhou, China) and then incubated with rabbit anti-TH antibody (1: 1000, AB152, Millipore, U.S.A.) overnight at 4 °C. On the second day, the sections were incubated with anti-

rabbit/mouse secondary antibodies kit (PV-9000, ZSGB-BIO, Beijing, China) for 30 min at 37 °C. After that, the sections were incubated with DAB (DAB-1031Kit, 20 ×, Maixin, Fuzhou, China) for 2 min and counterstained with hematoxylin for 1 min.

For the P<sub>Ser129</sub>αS staining, a previously published protocol was used [14-16]. The sections were treated with or without 50 µg/mL proteinase K (Aladdin, Shanghai, China) in 10 mM Tris-HCl, pH = 7.8, 100 mM NaCl, 0.1 % Tween-20 (Bio-Rad, U.S.A.) at 37 °C for 30 min. After that, sections were treated with 3% H<sub>2</sub>O<sub>2</sub> (5 min, Maixin, Fuzhou, China), 3% triton X-100 (4 min, Solarbio, Beijing, China), 10% goat serum (15 min, Maixin, Fuzhou, China) and incubated with a commonly used [14, 16-21] rabbit anti-P<sub>Ser129</sub>αS polyclonal antibody (1: 100, ab59264, Abcam, U.K.) overnight at 4 °C. On the second day, the sections were incubated with anti-rabbit/mouse secondary antibodies kit (PV-9000, ZSGB-BIO, Beijing, China) for 30 min at 37 °C. After that, sections were incubated with DAB (DAB-1031Kit, 20 ×, Maixin, Fuzhou, China) for 2 min and counterstained with hematoxylin for 1 min. To test the specificity of P<sub>Ser129</sub>αS staining, we used another classic rabbit monoclonal antibody for labeling P<sub>Ser129</sub>αS aggregates (ab51253, Abcam, U.K.) [12, 22]. The staining protocol was the same as described above but the antibody was changed to ab51253 (1:1000, Abcam, U.K.).

For the glial cells staining, astrocytes and microglia were stained in a standard way [23]. The sections were treated with 3% H<sub>2</sub>O<sub>2</sub> (5 min, Maixin, Fuzhou, China), 3% triton X-100 (4 min, Solarbio, Beijing, China), and 10% goat serum (15 min, Maixin, Fuzhou, China). For the astrocyte staining, the sections were incubated with mouse anti-GFAP antibody (1:1000, SMI21-R, Biolegend, U.S.A.) overnight at 4 °C. For microglia staining, the sections were incubated with rabbit anti-Iba1 antibody (1:500, 019-19741, Wako, Japan) overnight at 4 °C. After that, the sections were incubated with anti-rabbit/mouse secondary antibodies kit (PV-9000, ZSGB-BIO, Beijing, China) for 30 min at 37 °C. After that, sections were incubated with DAB (DAB-1031Kit, 20 ×, Maixin, Fuzhou, China) for 2 min and counterstained with hematoxylin for 1 min.

Hematoxylin and eosin (H & E) staining was used to identify the nigral pigmented cells (dopaminergic neurons) by the darkly stained hematoxylin and for staining the classical LBs with acidophilic inclusions. It was performed following the H & E kits instructions (G1120, Solarbio, Beijing, China). The brain sections were stained in the hematoxylin solution for 1 min and then washed with water. The sections were then treated with 1% hydrochloric acid-alcohol solution for 10

sec, washed back to blue and then stained in the eosin solution for 10 sec. After that, the sections were washed clean with water.

After the staining, all the sections were dehydrated with an alcohol gradient and xylene. Neutral balsam was used to cover the sections and digital pictures were taken with a microscope (Olympus, CX41; camera: Olympus DP25; software: CellSens Entry 1.4.1; Japan). For the three controls, the sections were stained in the same way.

Immunofluorescence staining was used to test the role of mutant LRRK2 *in vitro*. Cultured U251 cells stably expressing different LRRK2 mutations were fixed and stained with monoclonal antibody against serine 129-phosphorylated  $\alpha$ -synuclein (1:1000, ab51253, Abcam, U.K.). Immunoreactivity was detected with a FITC-conjugated secondary antibody (1:500, A-21207, invitrogen, U.S.A.) and nuclei were counterstained with DAPI and the slides were visualized under an Olympus FluoView™ 1000 confocal microscope (Olympus, U.S.A.).

#### ***e) Stereological (cell) counting***

After the immunostainings, stereological counting was carried out to quantify the pathological changes. The protocols were from previous reports [11, 13, 24, 25]. A typical immunostained section was screened under a 4 × objective (3.5 mm × 2.6 mm), a 20 × objective (690.8  $\mu$ m × 518.1  $\mu$ m) and a 40 × objective (345.4  $\mu$ m × 259  $\mu$ m) to locate the substantia nigra pars compacta (SNpc) for cell counting, because most nigral dopaminergic neurons are located in this area [9, 26]. The location of the counting frame on a section of the controls or the PD monkey candidate was at the same part of the SNpc, which was in the middle of the long axis of the SNpc (Figs. S10A-B, blue frame). This location was determined by both the anatomical characteristics of the SNpc (ellipsoid shaped and defined ventrally by the cerebral peduncle and medially by the third cranial nerve) and the cellular properties of the SNpc: pigmented cells (H & E staining in Fig. S10C), spindle-shaped cells (TH immunostaining in Fig. S10D) and their even distribution in the area (Fig. S10B).

The number of nigral dopaminergic neurons (TH<sup>+</sup> cells) in the area of the counting frame was counted by ImageJ software (National Institutes of Health, Bethesda, Maryland, USA) under the 40 × objective to ensure correct reorganization of the morphology of an individual cell (Fig. S10B, blue frame and zoomed in Fig. S10D). To quantify the nigral dopaminergic neuron loss in the PD monkey candidate, two additional age-matched normal control monkeys (ID: #071725 and #05103) were

interrogated with the DCMC to increase the statistical power. There were no significant differences in the SNpc dopaminergic neuronal count among the three control monkeys ( $P = 0.986$ , Chi-square test), and also no significant differences in the left and right side of SNpc of the three control monkeys ( $P = 1.00$ ,  $t$ -test). Therefore, the averaged density of cells (subjects/mm<sup>2</sup>) obtained from the left and right SNs of the controls (in total 18 sections containing the left and right SNs) were pooled together for statistics. For the PD monkey candidate, the dopaminergic neuron counting from both sides of the SNs (in total 6 sections containing the left and right SNs) was pooled together for no significant difference ( $P = 0.801$ ,  $t$ -test), and we found the averaged density of nigral dopaminergic neuron of the PD monkey candidate was close to that of PD patients [27].

To verify the reliability of the counting method, the total number of dopaminergic neurons in SNpc was estimated by a classic analysis method used in Garcia *et al.* [23] and Gundersen *et al.* [13]. The averaged total number of neurons in the SNpc of the three controls was around 13900, consistent with previous studies (around 14500) [11, 12], suggesting the counting was reliable. The stereological counting of the nigral P<sub>Ser129</sub>αS aggregates, microglia cells (nigral Iba1<sup>+</sup> cells) and astrocytes (nigral GFAP<sup>+</sup> cell) were carried out in the same way.

#### ***f) Dopamine concentration measurement***

The monkeys involved in this measurement (Table S1) were anesthetized with ketamine (10 mg/kg, 0.05 g/mL, i.m., Zhongmu, Taizhou, China). Approximately 1.5 mL CSF (divided into three 0.5 mL samples) of each monkey was collected with a lumbar puncture using a 22-gauge needle by an experienced technician. The collected CSF samples were immediately frozen in liquid nitrogen and stored at -80°C. Before the high-pressure liquid chromatography (HPLC) measurement, the CSF samples were thawed and centrifuged at 20000g for 15 min at 4 °C. Then, the dopamine (DA) concentration of each monkey was measured by HPLC (Antec 110, Holland) using an ALF-115 & ALF-105 column (Antec, Holland).

#### ***4) Genetic analysis and the related functional assays***

##### ***a) Gene sequencing***

Approximately 2 mL blood was collected from each of 1,585 cynomolgus monkeys for whole genome DNA extractions. Eleven PD risk / causal genes (*ATP13A2*, *FBXO7*, *GBA*, *GIGYF2*, *HTRA2*, *LRRK2*, *MAPT*, *PINK1*, *PLA2G6*, *SNCA*, and *UCHL1*) were selected for targeted

sequencing based on the severity of mutations previously published in PD exome sequencing studies [26, 28, 29]. An improved algorithm, MIPgen [30] was used to design molecular inversion probes (MIPs), which are single stranded DNA molecules containing two regions complementary to regions in the targeted DNA [31-33]. For the 11 targeted genes, the final probe designs included 359 smMIPs. Oligonucleotides were obtained from Integrated DNA Technologies (IDT, Coralville, IA, USA). MIPs were pooled by gene. The MIPs, 100 ng genomic DNA, 0.32 mM dNTPs, 0.32  $\mu$ L Hemo KlenTaq (New England Biolabs, Inc., Ipswich, MA, USA) and 1 unit of Ampligase (Epicentre) were mixed with 1  $\times$  Ampligase buffer (Epicentre, Madison, WI, USA) in a PCR tube with a total reaction volume of 25  $\mu$ L. Gap filling and ligation were also performed in the same PCR tube. The PCR tubes were incubated at 95°C for 10 min and then 60°C for 22 h. Subsequently, 2  $\mu$ L exonuclease mix was added into the same tube and incubated at 37°C for 45 min and then 95°C for 2 min. The captured DNA was amplified as previously reported [34] and 5  $\mu$ L amplified products were pooled together and purified with 0.9  $\times$  AMPure XP beads (Beckman Coulter, Brea, CA, USA) according to standard protocol. Then gel visualization with 2% agarose gel and quantification with the Qubit dsDNA HS Assay (Life Technologies, Grand Island, NY, USA) were performed. Approximately 384 individuals were combined as the final pool for sequencing in one lane of an Illumina HiSeq 3000. The sequences were mapped to RheMac3 (<http://genome.ucsc.edu/cgi-bin/hgGateway?db=rheMac3>) using BWA-MEM [35]. For quality control, read pairs with incorrect pairs and insert sizes were removed after mapping, leaving only the reads with the highest quality scores. FreeBays [30] was applied for variant calling and SeattleSeq138 (<https://snp.gs.washington.edu/SeattleSeqAnnotation137>) for variants annotation. For the validation of variants, 300 bp primers were designed using BatchPrimer3 (<https://wheat.pw.usda.gov/demos/BatchPrimer3>). PCR was performed with a standard program in 25  $\mu$ L reaction volume. The PCR products were mixed and purified with 0.9  $\times$  AMPure XP beads and the product was sent for Sanger sequencing.

The MIP sequencing information for PD-risk / causal genes in the spontaneous PD monkey and Combined Annotation Dependent Depletion (CADD) score [36, 37] is listed in Table S3.

### ***b) Construction of U251 cells with stable LRRK2 mutant expression***

We performed cellular assays to characterize the potential effect of the LRRK2 mutants p.E2381G,

p.N1506Y and p.I835L. We generated three mutants (p.E2381G, p.N1506Y and p.I835L) based on the wild type (WT) LRRK2-pCMV-c-Myc vector, constructed in our previous study [38], by using site-directed mutagenesis PCR methods. All mutants were verified by sequencing. All primer information is shown in Table S4.

To generate a stable and inducible cell line expressing WT or mutant LRRK2 upon doxycycline (Dox, Sigma, St Louis, MO, U.S.A.) induction, we used Lenti-X Tet-On Advanced Inducible Expression System (Clontech) following our previously reported method [38]. In brief, WT or mutant LRRK2 was subcloned into pLVX-tight-puro (Clontech) by using two sets of primers to introduce restriction endonuclease sites (*NotI* and *MluI*) and the c-Myc tag (Table S4). The response lentivirus system was composed of WT or mutant LRRK2 constructs, packaging plasmid psPAX2 (12260, Addgene, U.K.) and envelope plasmid PMD2.G (12259, Addgene, U.K.), while the regulator lentivirus system was composed of PLVX-Tet-On-Advanced vector, psPAX2 and PMD2.G. The HEK293T cells were introduced from the Kunming Cell Bank, Kunming Institute of Zoology, and were cultured in DMEM (11965, Gibco, U.S.A.) containing 10% heat inactivated FBS. Cells were transfected with LRRK2 or Advance vector, packaging plasmid psPAX2 and envelop plasmid PMD2.G with a ratio of 3:2:1. The lentivirus was collected from cell supernatant at 48 h after transfection. The U251 cells were maintained in RPMI 1640 supplemented with 10% FBS (11875, Gibco, U.S.A.). The lentivirus supernatant was produced from HEK293T cells and was used to infect U251 cells with the ratio of 4:1 for the response lentivirus and the regulator lentivirus. Cells were selected in growth medium with 500 µg/mL G418 and 2 µg/mL puromycin for 2 weeks. Control U251 cells, U251 cells with pLVX-tight-puro (Clontech) and U251 cells with LRRK2 were cultured in a 6-well plate with 2 µg/mL doxycycline (Sigma) for 48 h to induce LRRK2 protein expression.

### ***c) Western blotting***

The U251 cells stably expressing different LRRK2 mutants were harvested for Western blot and RNA-seq. Total cellular protein was obtained by using cell lysis buffer (P0013, Beyotime, China) and the protein concentration was determined by BCA Protein Assay Kit (P0012, Beyotime, China). Western blots were performed using the method described in our previous studies [39, 40]. In brief, 30 µg protein was separated by 10–15% sodium dodecyl sulfate-polyacrylamide gel electrophoresis, transferred to a polyvinylidene difluoride membrane (Bio-Rad, Hercules, CA, U.S.A.) and the

membrane was blocked with 5% (w/v) skim milk for 2 h at room temperature. The membrane was then incubated with the respective primary antibody against c-Myc (1:1000, C3956, Sigma, U.S.A.), LRRK2 (1:1000, ab133518, Abcam, U.K.), p-LRRK2<sup>Ser1292</sup> (1:1000, ab203181, Abcam, U.K.), RAB10 (1:1000, ab181367, Abcam, U.K.), p-RAB10<sup>Thr73</sup> (1:1000, ab231707, Abcam, U.K.), and tubulin (1:10000, E1c601, EnoGene, U.S.A.) overnight at 4°C. The membranes were washed 3 times with Tris-buffered saline/Tween 20 for 5 min, followed by incubation with the peroxidase-conjugated anti-mouse (474-1806) or anti-rabbit (474-1516) IgG (1:5000; KPL) antibody for 1 h at room temperature. The signal was visualized using an ECL western blot detection kit (Millipore, WBKLS0500). ImageJ (National Institutes of Health, Bethesda, Maryland, USA) was used to evaluate the densitometry data. Western blot for tubulin was used as a loading control.

#### ***d) RNA extraction and RNA sequencing (RNA-Seq)***

Total RNA was isolated from tissues and cell lines using TRIZOL (Invitrogen, 15596-018) according to the manufacturer's instructions. RNA-Seq for mRNA expression profiling of the U251 cells with a stable expression of LRRK2 was performed using the method described in our previous study [41]. In brief, about 1 µg total RNA per sample was used to prepare library for RNA-seq. Sequencing libraries were generated using the NEBNextUltra™ RNA Library Prep kit from Illumina (NEB, USA) following the manufacturer's recommendation and index codes were added to attribute sequence to each sample. The processed final library was sequenced on an IlluminaHiSeq 4000 platform, and 150 bp paired ends reads were generated. Raw RNA-seq reads were trimmed to remove sequencing adapters and low-quality reads. The clean reads were then aligned to the reference genome (GRCh38.p7) using HISAT2 [42]. FeatureCounts was used to generate counts for known genes [43]. Gene-level differential expression analyses were performed using DESeq2 [44]. Gene Ontology enrichment analysis of target gene sets was analyzed by DAVID 6.8 (<https://david.ncifcrf.gov>) [45].

#### ***Statistical analysis***

Nonparametric statistics (Mann-Whitney) was used to compare the means/distributions of the total PD score and score of each item in the spontaneous PD monkey and the three control monkeys before and after L-dopa or apomorphine treatment. Nonparametric statistics (Mann-Whitney) was

used to compare the means/distributions of the counting data from nigral TH cells, P<sub>Ser129</sub>αS aggregations, microglia cells, and astrocytes. The means/distributions of the TH cells in left and right side SNs were analyzed by the Student's *t*-test. The linear regression between dopamine concentration of CSF samples and the ages of the monkeys was performed by Correlations-double variant & Regression-Curve fit. ANOVA (homogeneous variance) was used to compare the means/distributions of Iba1 labeled microglia's soma diameter. ANOVA with the Tukey's post-hoc test (homogeneous variance) was used to compare the means/distributions of the relative levels of protein expression in Western blot.

## Supplementary Results

### *Identification of the PD risk gene mutations in the Spontaneous PD monkey*

It has been well established that PD, especially early-onset PD, has a significant genetic contribution [26, 46, 47]. Because our spontaneous PD monkey represents an early-onset PD case (a 10-year old monkey is approximately equal to a 30-40 years old human being [48, 49]), we subjected the PD monkey and 1,585 cynomolgus monkey controls to a genetic screen by sequencing the coding regions of 11 human PD risk genes (*ATP13A2*, *FBXO7*, *GBA*, *GIGYF2*, *HTRA2*, *LRRK2*, *MAPT*, *PINK1*, *PLA2G6*, *SNCA* and *UCHL1*). In total, 14 missense mutations were found among 6 genes of the spontaneous PD monkey compared to a population of 1,585 cynomolgus monkey controls (Table S3). Subsequently, the identified *LRRK2* and *ATP13A2* rare mutations were verified by Sanger sequencing, and the mutation locations were clearly delineated (Fig. S5).

A sequence alignment of multiple species was conducted to determine if the *LRRK2* mutation sites were conserved during evolution. The alignment indicated that the three *LRRK2* missense mutation sites represented nucleic acid base substitutions in highly conserved loci (Fig. S6) in three functional domains. These included Ankyrin repeats (ANK) that are part of transcription factors and signaling proteins; Ras protein of the GTPase complex (Roc-GTPase), potential regulators of *LRRK2* kinase activity, and WD40 domains, the most common repeats in human proteins and found in functionally diverse proteins, such as G protein subunits, protein phosphatase subunits, and RNA processing complexes [50]. Therefore, the identified missense mutations are part of functional domains that may impact *LRRK2* function and promote PD pathogenesis (Fig. S5A). Although the PD monkey *LRRK2* mutations are not the same to humans, their location is close to the ones identified in PD patients [51]. The fact that they are non-synonymous mutations which result in amino acid changes makes it very likely that they affect *LRRK2* functions. In addition, the identified CADD score  $\geq 15$  is another indicator of a conserved site (Table S3) with a possibly high impact for disease [36, 37]. We also found and verified another missense mutation in the *ATP13A2* gene (Fig. S5B). The *ATP13A2* protein is required for normal lysosome function to prevent  $\alpha$ -synuclein aggregation in neurons [52, 53].

The sequencing results supported the genetic basis [54, 55], and suggested that a potential dysfunction of *LRRK2* and *ATP13A2* might contribute to the observed spontaneous PD monkey

phenotype. Interestingly, we confirmed that all missense mutations in the spontaneous PD monkey were not present in his available family members including the elder sister (#04106) and father (#95111). Moreover, a behavioral assessment of the elder sister and the father revealed no typical PD symptoms in both animals.

### ***The PD-associated LRRK2 mutations in the spontaneous PD monkey have functional consequences***

The next question we asked was whether the *LRRK2* mutations we found in the spontaneous PD monkey can in fact explain PD-related pathology. We focused on the *LRRK2* variants and included the verified *LRRK2* mutant p.G2019S that has been identified in PD patients as a positive control. The three *LRRK2* mutants (p.E2381G, p.N1506Y and p.I835L) identified in the spontaneous PD monkey were generated by using site-directed mutagenesis on the wild type (WT) *LRRK2*-pCMV-c-Myc vector constructed in our previous study [38] and were verified by sequencing (Table S4). HEK293T cells were then transfected and the lentivirus supernatant produced from HEK293T cells was used to infect U251 cells.

Western blots confirmed stable expression of mutant *LRRK2* proteins (Fig. S7A). We then analyzed potential markers relevant for *LRRK2* function and PD pathogenesis (Fig. S7B). We found that serine 1292-phosphorylated *LRRK2* (p-Ser1292 *LRRK2*) and threonine 73-phosphorylated Rab10 (p-Thr73 Rab10) levels were both increased (Fig. S7C). We speculate that the increased *LRRK2* phosphorylation and Rab10 phosphorylation may contribute to PD pathogenesis of the spontaneous PD monkey. This is based on previous findings that have shown that phosphorylated Rab10 can be activated by *LRRK2*-mediated phosphorylation to trigger PD pathogenesis [51, 56].

To get a comprehensive understanding regarding the potential role of the *LRRK2* mutants, we performed RNA sequencing (RNA-Seq) and found that many genes were differentially expressed in *LRRK2* mutant overexpressing cells compared to controls (positive control p.G2019S: 26 genes; p.N1506Y: 142 genes; p.E2381G: 58 genes, and p.I835L: 663 genes) (Fig. S7D). Affected pathways of three *LRRK2* mutants were related to immunologic dysfunction (Fig. S7F-H), which is one of the current mainstream hypothesis of PD pathogenesis. Collectively, the RNA-Seq analysis data indicated that activated immunologic reactions or inflammations may contribute to PD pathogenesis

in the spontaneous PD monkey, which is also consistent with the glial cell activation we observed.

To further confirm the pathological changes induced by the *LRRK2* mutants in U251 cultured cells, we selected P<sub>Ser129</sub> $\alpha$ S as a pathology marker for immunofluorescence staining. We found that P<sub>Ser129</sub> $\alpha$ S is expressed and accumulated at high levels in all *LRRK2* mutant cells compared with wild type and PLVX control cells and with most of the protein located in the cytoplasm (Fig. S8). This finding was consistent with the  $\alpha$ -synuclein pathology that we had found in the spontaneous PD monkey.

The functional tests *in vitro* suggested that the *LRRK2* mutations we found in the spontaneous PD monkey can at least partially explain its PD-related pathology.

## Supplementary Figures

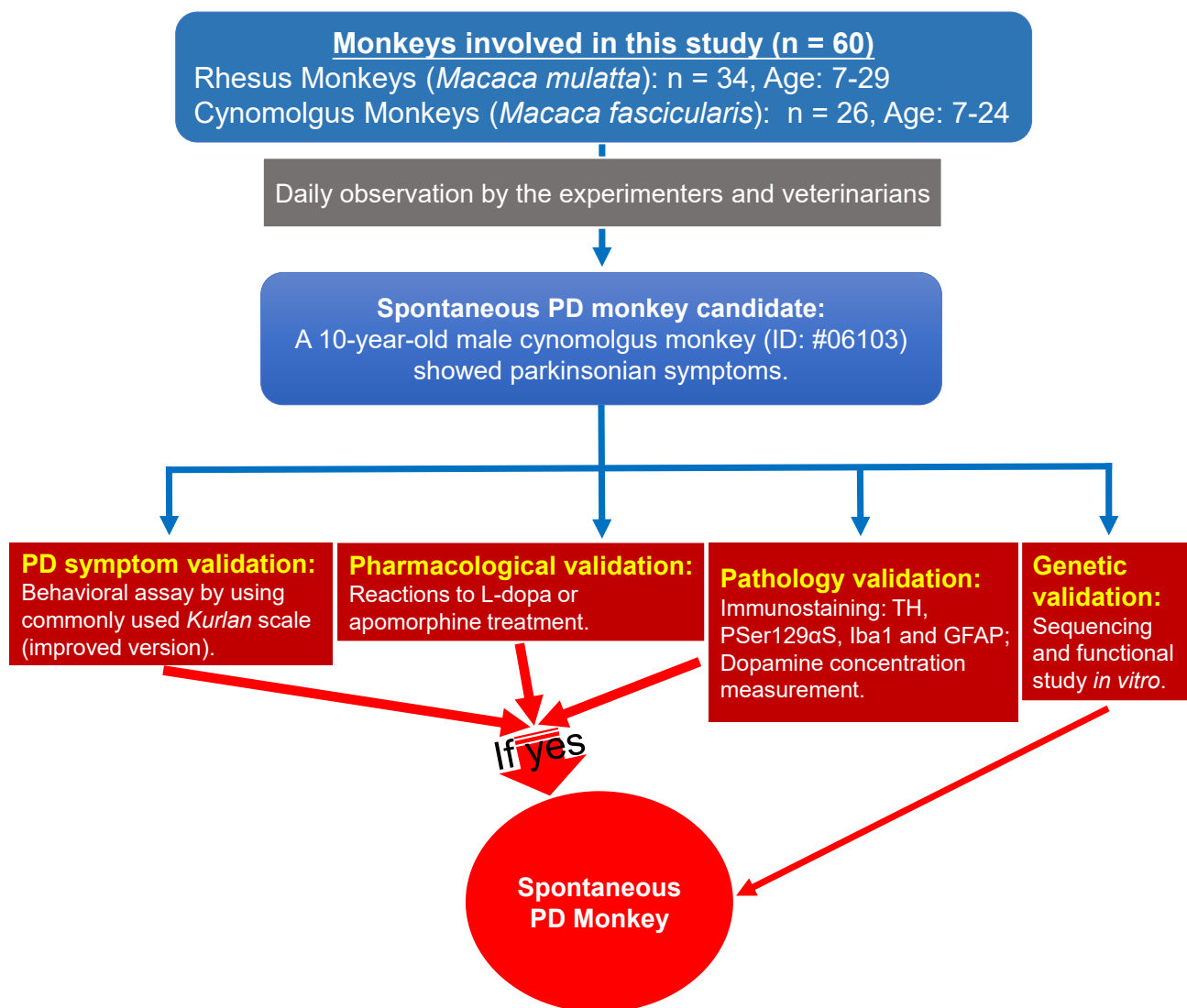


**Figure S1.** A flow chart shows the search process (blue and gray panel) and four validation steps (red panels) used in the screening of spontaneous PD monkey candidates.

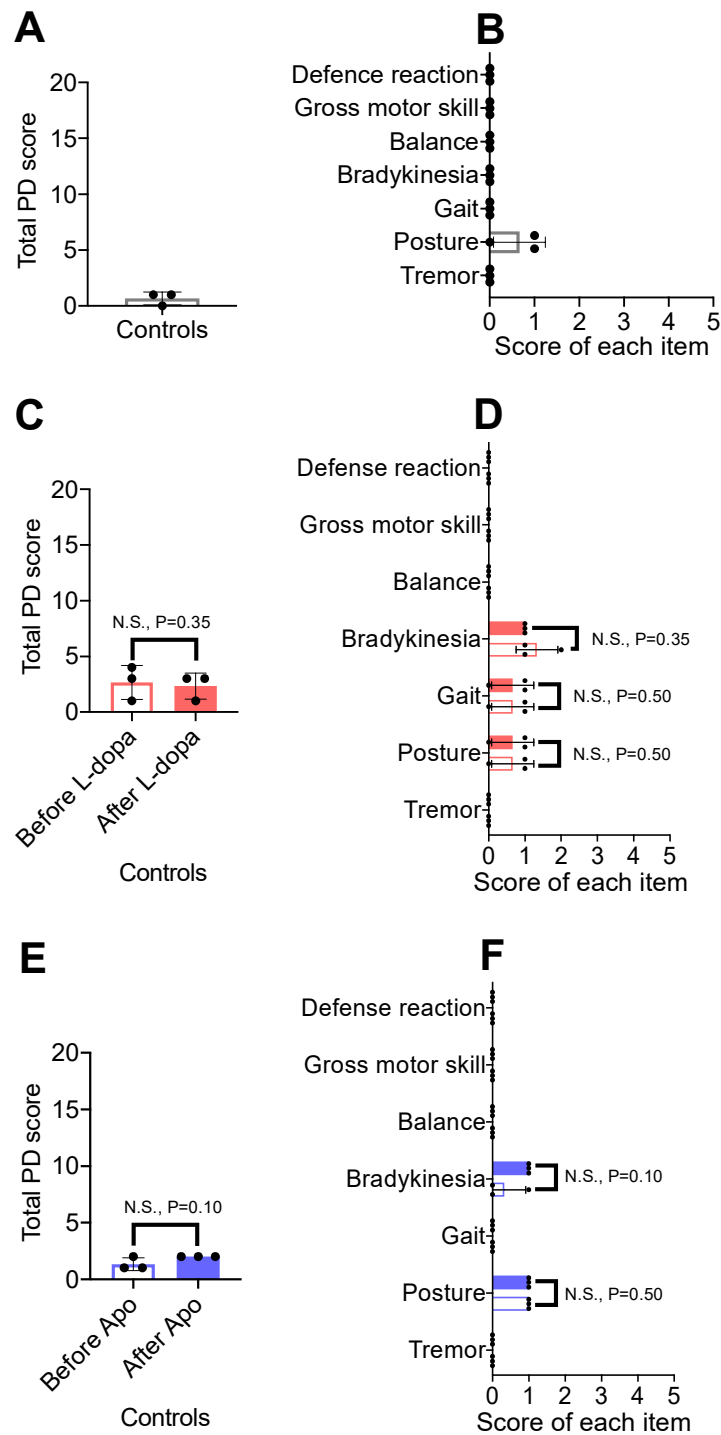
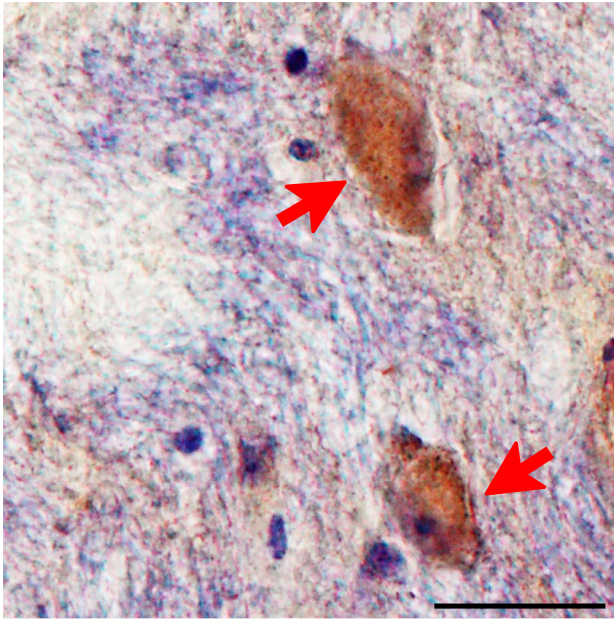


**Figure S2.** PD symptom assessment of the three control monkeys. **(A)** Quantified by the improved *Kurlan* scale, the averaged total PD score of the controls was around 1, which was within the normal range according to the scale (0 to 4). **(B)** Seven items that make up the scale were marked zero except for the posture, which was less than 1. **(C)** The averaged total PD score of the controls was not significantly changed after the L-dopa treatment. **(D)** The seven items were not significantly changed after the L-dopa treatment. **(E)** The averaged total PD score of the controls was not significantly changed after the Apo treatment. **(F)** The seven items were not significantly changed after the Apo treatment. Data are means  $\pm$  SD. Nonparametric statistics (Mann-Whitney test) was used. N.S., not significant.

ab59264 (1:100)



ab51253 (1:1000)

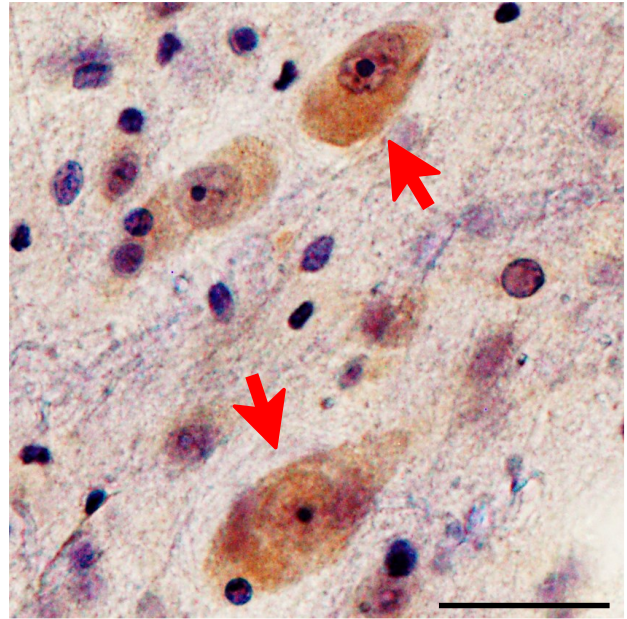


**Figure S3.** Comparison of two antibodies staining of phosphorylated-Ser129  $\alpha$ -synuclein (P Ser129  $\alpha$  S) in locus ceruleus (LC) of the spontaneous PD monkey. The rabbit polyclonal antibody (ab59264, 1: 100) and the rabbit monoclonal antibody (ab51253, 1: 1000) can both stain the P Ser129  $\alpha$  S aggregates (red arrows). The results obtained from both are similar. Scale bar: 20  $\mu$ m.

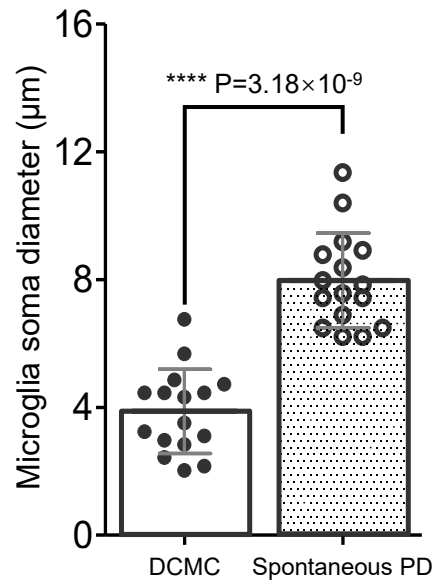


**Figure S4.** The average soma diameters of microglia in the spontaneous PD monkey (ID: #06103) were significantly larger than that of the death-condition-matched control (DCMC, ID: #071809). For each monkey, one section (section #34) was picked. The location of the counting frame under a 40 × objective was similar to that of nigral dopaminergic neurons quantification, from which 16 typical Iba1<sup>+</sup> cells were selected for measuring the soma diameter by ImageJ software. Data are means ± SD. One-way ANOVA was used for the statistics.

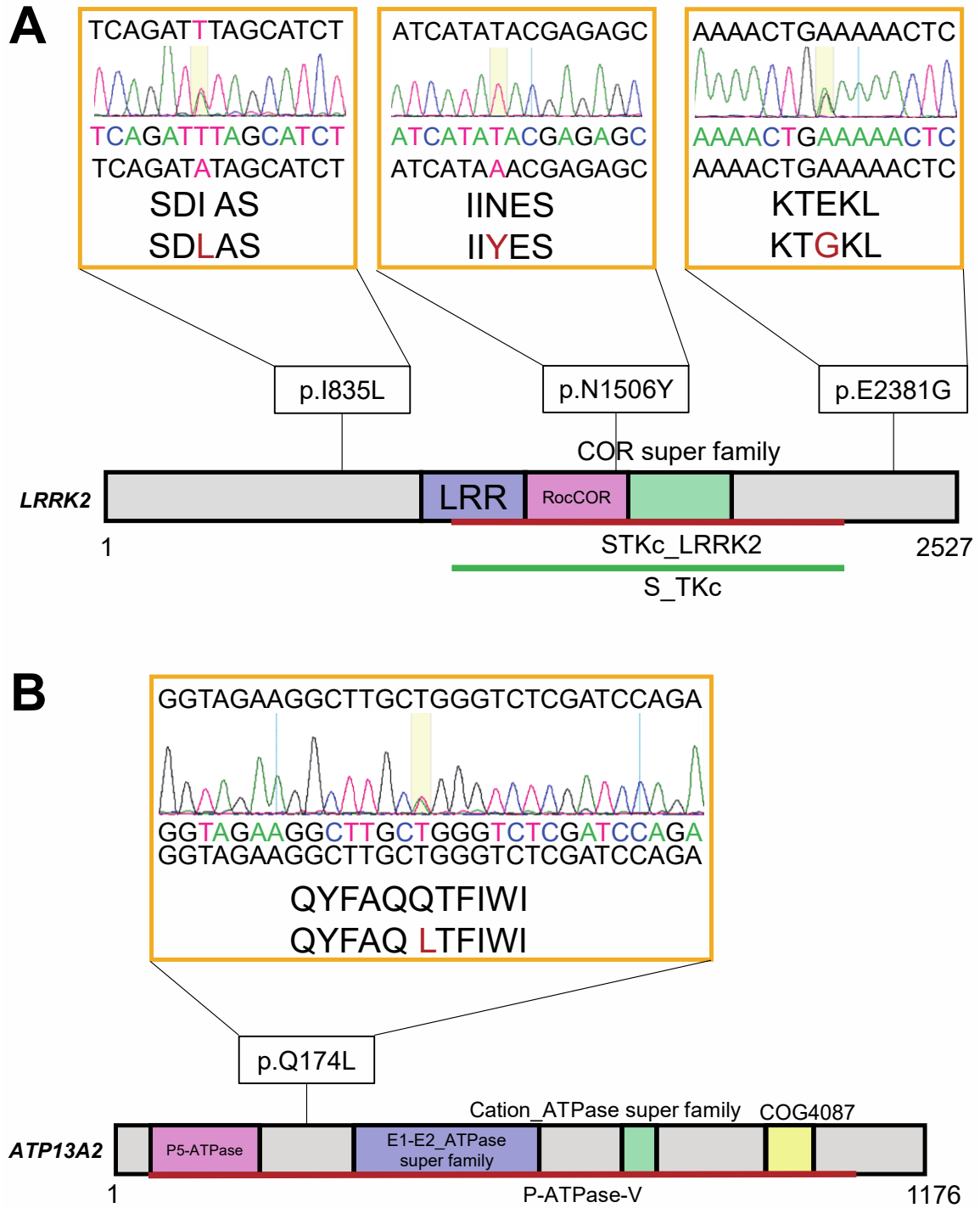


**Figure S5.** The LRRK2 and ATP13A2 missense mutations of the spontaneous PD monkey. **(A)** Sequencing verification of the LRRK2 mutations. **(B)** Sequencing verification of the ATP13A2 mutation.

Species of primates	DNA sequence comparisons of three missense mutations in LRRK2		
	c.2503A>T	c.4516A>T	c.7142A>G
Human	CAGATATAGCA	TCATAAACGAG	AACTGAAAAAC
<b>Macaque (#06103)</b>	CAGAT <b>T</b> TAGCA	TCATA <b>T</b> ACGAG	AACTG <b>G</b> AAAAC
Chimpanzee	CAGATATAGCA	TCATAAACGAG	AACTGAAAAAC
Gorilla	CAGATATAGCA	TCATAAACGAG	AACTGAAAAAC
Orangutan	CAGATATAGCA	TCATAAACGAG	AACTGAAAAAC
Marmoset	CAGATATAGCA	TCATAAACGAG	AACTGAAAAAC
Gibbon	CAGATATAGCA	TCATAAACGAG	AACTGAAAAAC

**Figure S6.** Alignment of primates *LRRK2* gene sequences. The missense mutations of *LRRK2* identified in the spontaneous PD monkey (ID: #06103) were compared with 6 other primate species.

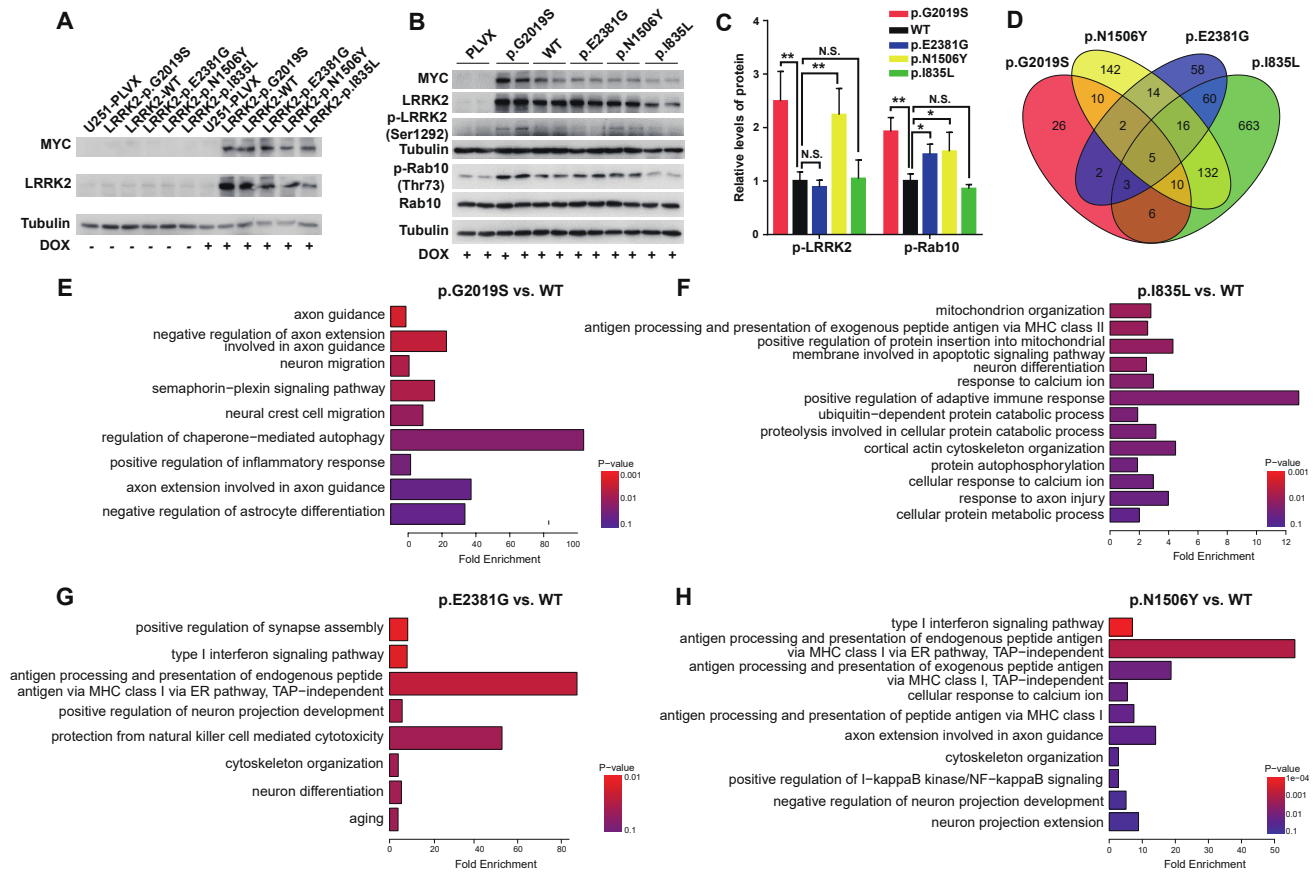


**Figure S7.** Functional characterization of the LRRK2 mutants identified in the spontaneous PD monkey. **(A)** Immunoblot analysis of total U251 cell lysates with stable expression of wild type (WT) and mutant LRRK2 induced by doxycycline (2  $\mu\text{g}/\text{mL}$ ) treatment. **(B)** Protein levels of LRRK2, p-LRRK2, p-Rab10, and Rab10 in U251 cell lysates with stable expression of wild type and mutant LRRK2 in the presence of doxycycline. **(C)** Densitometry of the proteins in figure **(B)**. Relative protein abundance was normalized to tubulin. Data is representative of 3 independent experiments with similar results. \*,  $P < 0.05$ ; \*\*,  $P < 0.01$ ; N.S., not significant. One-way ANOVA with the Tukey's post-hoc test was used. Data in figure **(C)** are means  $\pm$  SD. **(D-H)** Differentially expressed genes (DEGs) and disrupted pathways of DEGs in U251 cells with stable expression of different LRRK2 mutants induced by doxycycline (2  $\mu\text{g}/\text{mL}$ ) treatment. **(D)** Total number of differentially expressed genes. **(E-H)** Enriched pathways in U251 cells with stable expression of LRRK2 mutations p.G2019S **(E)**, p.I835L **(F)**, p.E2381G **(G)**, and p.N1506Y **(H)**, relative to wild type (WT) LRRK2. Enriched biological processes in Gene Ontology (GO) of the target gene sets were identified by DAVID 6.8 (<https://david.ncifcrf.gov>) [45]. Shown are enriched terms with  $P < 0.05$ ; x-axis, fold enrichment; y-axis, enriched GO terms.

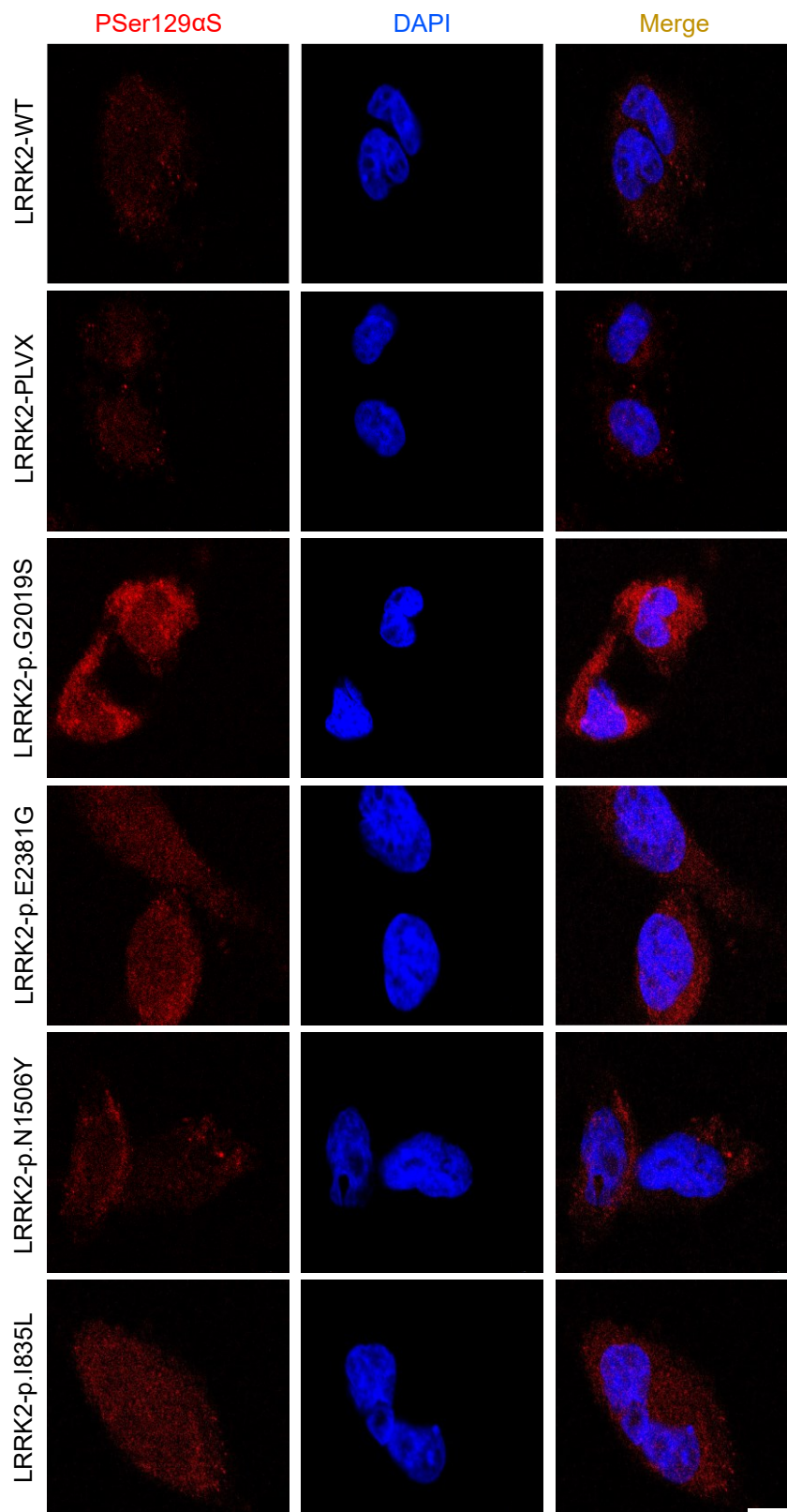


**Figure S8.** Effect of different LRRK2 mutants on the formation of intracellular PSer129 $\alpha$ S aggregates in U251 cells using immunofluorescence. Data are representative of three independent experiments with similar results. Scale bar: 10  $\mu$ m.

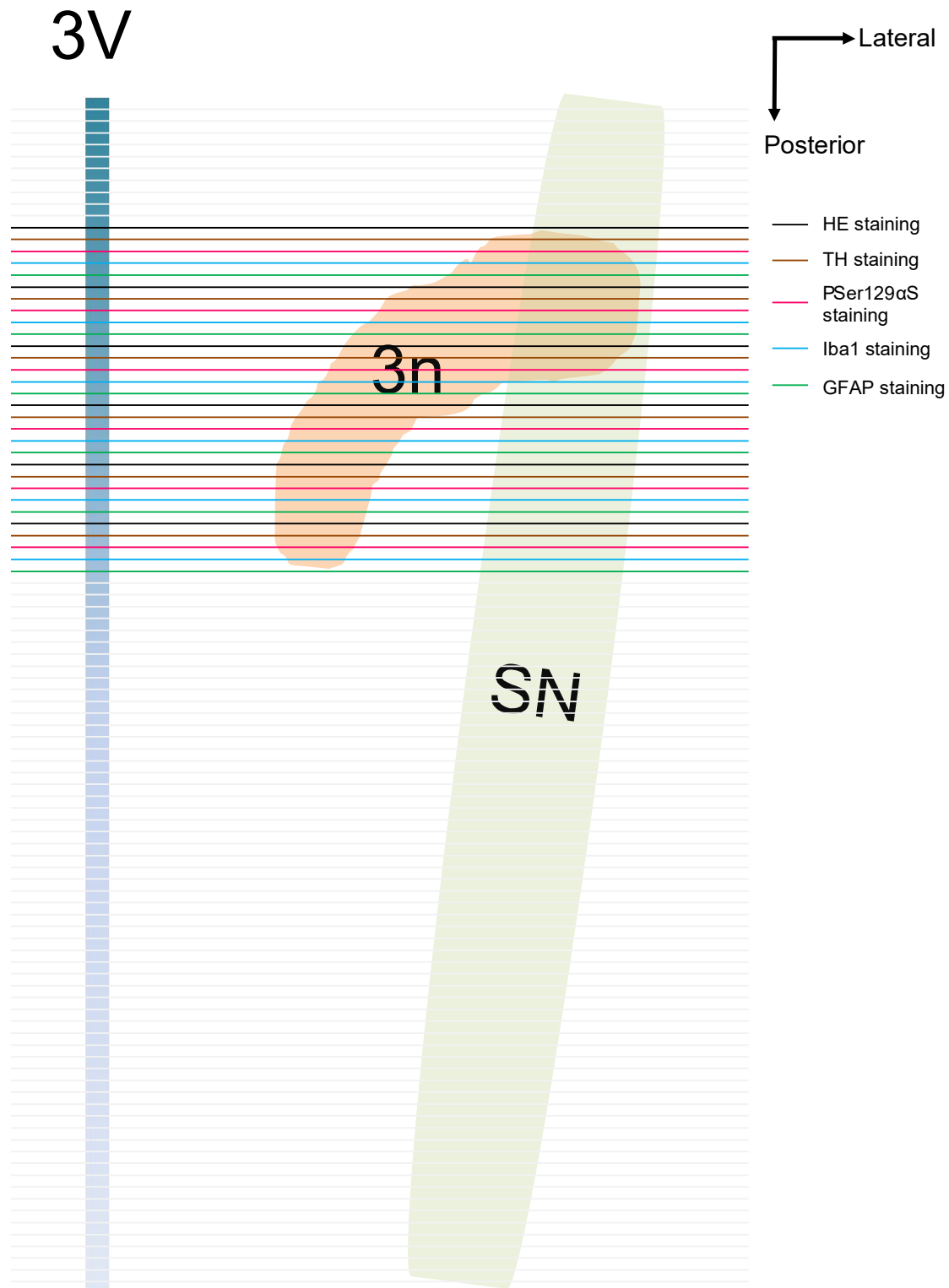


**Figure S9** Diagram illustrating how the 30 optimal sections of a monkey's right substantia nigra (SN) were divided into six sets for HE, TH, P-ser 129  $\alpha$ -Syn, Iba1 and GFAP staining, respectively. Each set has 5 sections, which are marked with five lines in specific colors. A monkey's SN was sectioned into 100 sections with an interval of 60  $\mu$ m in between. Each line represents one section within a thickness of 20  $\mu$ m. The 30 sections overlapped with the 3n are optimum for nigral dopaminergic cell counting [9]. 3n: the third nerve, 3V: the third ventricle.

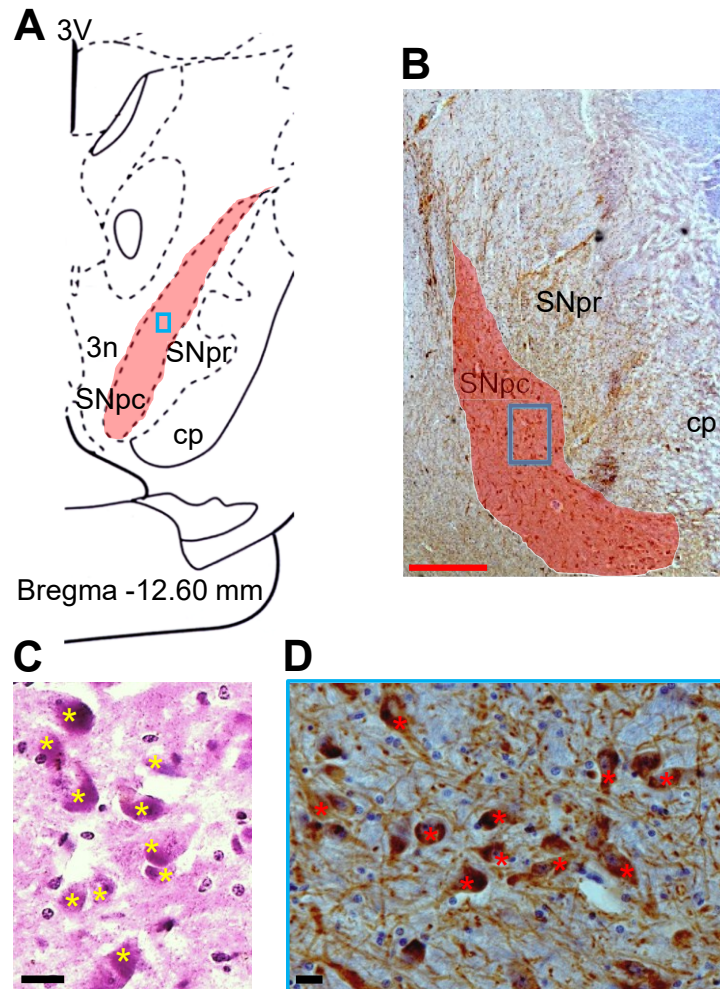


**Figure S10.** Based on the SNpc anatomical and dopaminergic neuron morphological features, the location of a counting frame for stereological counting in a substantia nigra (SN) section of the death-condition-matched control (DCMC) was determined. **(A)** A diagram of a monkey's SN and related structures modified from "*The Rhesus Monkey Brain in Stereotaxic Coordinates*, George Praxinos et al., Academic Press, 1999". The red shaded area shows the whole unilateral SNpc and the location of a blue counting frame, which is in the middle of the long axis of the SNpc. The area inside the blue frame is for the counting of dopaminergic neurons. **(B)** A nigral TH immunostaining image of the DCMC under a  $4\times$  objective ( $3.5\text{ mm} \times 2.6\text{ mm}$ ). The red shaded area shows the whole unilateral SNpc and the blue counting frame in the middle of the SNpc shows the area for cell counting. **(C)** Nigral pigmented cells marked with yellow asterisks in a H & E image under a  $40\times$  objective ( $345.4\ \mu\text{m} \times 259\ \mu\text{m}$ ). **(D)** Spindle-shaped nigral dopaminergic neurons marked with red asterisks in a TH immunostaining image under a  $40\times$  objective. This is the area in the blue frame of figure **(B)**. Both **(C)** and **(D)** show the dopaminergic neuron morphological features for determining the location of the counting frame in the SNpc: clear and evenly distributed dopaminergic neurons in the area, which is indicated by both HE staining and TH immunostaining in **(C)** and **(D)**, respectively. After careful comparison, we assumed the location of the blue counting frame should be in the middle of the long axis of the SNpc, and this location was applied to all the 30 optimum sections. Scale bars: red:  $500\ \mu\text{m}$ , black:  $20\ \mu\text{m}$ . 3n: the third cranial nerve; 3V: the third ventricle; cp: the cerebral peduncle; SNpc: substantia nigra pars compacta; SNpr: substantia nigra pars reticulata.

## Supplementary Tables

**Table S1.** Detailed information of the 60 monkeys involved in the study. The 60 monkeys were selected from the colonies (2,400+ individuals) at the Kunming Primate Research Center, Kunming Institute of Zoology, Chinese Academy of Sciences. The spontaneous PD monkey (ID: #06103) is labeled in red. A death-condition-matched control (DCMC, ID: #071809) is labeled in gray, and two age-matched control monkeys (ID: #071725 & #05103) are labeled in blue. The eight monkeys labeled in green were normal controls for CSF dopamine concentration test. \*indicates age of each monkey that was part of the study.

Rhesus monkey (n = 34)			Cynomolgus monkey (n = 26)		
ID: #	Age*	Gender	ID: #	Age*	Gender
070141	9	Male	06101	10	Male
060113	10	Male	06103	10	Male
090019	7	Male	95111	24	Male
705351	9	Male	04106	14	Female
070209	9	Male	080011	8	Male
070155	9	Male	071725	9	Male
070229	9	Male	05103	11	Male
080227	8	Male	071809	9	Male
070179	9	Male	080009	8	Male
06411	10	Male	08103	8	Male
06415	10	Male	071023	9	Male
07451	9	Male	071905	9	Male
08005	8	Male	080015	8	Male
08031	8	Male	071069	9	Male
08301	8	Male	08101	10	Male
08377	8	Male	00107	18	Male
08419	8	Male	04107	14	Male
91327	25	Male	04109	14	Male
93334	23	Female	060245	12	Male
94354	22	Female	11133	7	Male
94356	22	Female	08105	8	Male
89323	27	Male	97101	21	Male
93332	23	Female	09103	9	Male
89313	27	Male	11137	7	Male
91319	25	Male	051090	11	Female
90309	26	Male	060309	12	Male
92348	24	Female			
92350	24	Female			
92330	24	Female			
91313	25	Male			
89325	27	Male			
90319	26	Male			
94338	22	Female			
87033	29	Male			

**Table S2.** Improved version of the *Kurlan* scale (*A Monkey-Parkinsonism Rating Scale*). The part A and part D are listed.

---

**Part A. Parkinsonian features (20 scores in total)**

---

**1. Tremor (L/R):** like the tremor of PD patients

- 0-absent
- 1-slight-low amplitude and only intermittently present
- 2-moderate-moderate amplitude and present most of the time
- 3-severe-high amplitude, virtually continuous, interferes with function

**2. Posture:** different from the postural instability of PD patients, not applicable to PD patients

- 0-normal, erect
- 1-stooped
- 2-face down

**3. Gait:** partly like the postural instability of PD patients

- 0-normal, use all four limbs smoothly
- 1-walks slowly
- 2-marked impaired, able to ambulate but very slowly and with effort
- 3-severe decrease in ability to ambulate
- 4-unable to ambulate

**4. Bradykinesia (generalized):** like the bradykinesia of PD patients

- 0-normal speed and facility of movement
- 1-mild slowing of overall movements
- 2-moderate slowing of movements
- 3-severe slowing of movements: slow, labored, and difficult to initiate and maintain movement
- 4-unable to ambulate

**5. Balance:** partly like the postural instability of PD patients

- 0-normal balance
- 1-mild loss of balance on arising or with movement, holds onto cage for support
- 2-major lapse in balance

**6. Gross motor skills (upper limb, L/R):** partly like the postural instability of PD patients

- 0-normal, uses limb through a wide range of motion and activities
- 1-noticeable decrease in capacity to use limb, but used consistently
- 2-severe decrease in capacity to use limb, rarely used
- 3-unable or refuses to use limb (including walking)

**7. Defense reaction (defensive and/or aggressive response to examiner):** not applicable to PD patients

- 0-normal, reacts appropriately
- 1-detectable impaired, slowed, abnormal or shortened response
- 2-little or no response upon good provocation

---

**Part D. Clinical staging (5 stages)**

- I. Hemi-Parkinsonism, uses affected upper limb for walking
- II. Hemi-Parkinsonism, does not use affected upper limb for walking
- III. Bilateral Parkinsonism, maintains adequate nutrition without assistance
- IV. Bilateral Parkinsonism, requires assistance to maintain adequate nutrition, maintains upright position
- V. Bilateral Parkinsonism, requires assistance to maintain adequate nutrition, face-down position

---

**Note:**

Part A was used to determine the Parkinsonian score while part D provided clinical measures of the Parkinsonian stage [2].

**Table S3.** MIP sequencing information for PD-risk / causal genes in the spontaneous PD monkey (ID: #06103). Combined Annotation Dependent Depletion (CADD) was used as a tool for scoring the effect size of single nucleotide variants [36, 37]. A CADD score  $\geq 15$  is an indicator of conserved sites, which could possibly have a high impact on PD pathogenesis.

Chromosome	Position	Reference Base	Sample Genotype	Sample Alleles	Function GVS	Amino Acids	Protein Position	cDNA Position	Chimp Allele	Gene List	Protein Sequence	CADD Scores
12	40704431	A	T	T/T	missense	ASN, TYR	1506/2528	4516	A	LRRK2	NP_940980.3	21.3
22	38508211	C	T	T/T	missense	ARG, HIS	739/753	2216	C	PLA2G6	NP_001004426.1	12.54
2	233655834	T	G	G/G	missense	ASP, GLU	349/1300	1047	T	GIGYF2	NP_001096616.1	10.43
1	155209708	C	T	T/T	missense	MET, ILE	92/537	276	C	GBA	NP_000148.2	7.153
1	17328861	C	T	T/T	missense	ASP, ASN	184/1176	550	C	ATP13A2	NP_001135445.1	18.21
22	38541638	C	Y	C/T	missense	ALA, THR	78/753	232	C	PLA2G6	NP_001004426.1	10.25
12	40757317	A	R	A/G	missense	GLU, GLY	2381/2528	7142	A	LRRK2	NP_940980.3	20.8
1	17316247	C	Y	C/T	missense	VAL, ILE	845/1176	2533	C	ATP13A2	NP_001135445.1	11.55
4	41259691	G	S	C/G	missense	GLU, ASP	37/224	111	G	UCHL1	NP_004172.2	12.39
1	17330848	T	W	A/T	missense	GLN, LEU	174/1176	521	T	ATP13A2	NP_001135445.1	12.44
1	17331258	C	Y	C/T	missense	ALA, THR	136/1176	406	C	ATP13A2	NP_001135445.1	10.28
1	155209520	A	R	A/G	missense	PHE, SER	114/537	341	A	GBA	NP_000148.2	11.54
1	155209489	C	Y	C/T	missense	MET, ILE	124/537	372	C	GBA	NP_000148.2	14.03
12	40681155	A	W	A/T	missense	ILE, LEU	835/2528	2503	A	LRRK2	NP_940980.3	8.162

**Table S4.** Primers for cloning and site mutagenesis of the *LRRK2* gene.

Primer <sup>a</sup>	Sequence (5'-3')	Application
<b>For site mutation</b>		
p.E2381G-F	GGGATAAGAAAAC <u><b>G</b></u> GAAAACCTCTGTGGAC	Mutant E2381G-LRRK2
p.E2381G-R	GTCCACAGAGTTTT <u><b>C</b></u> AGTTTTCTTATCCC	
p.N1506Y-F	CGGAAAACCATCA <u><b>T</b></u> ATACGAGAGCCTTAAT	Mutant N1506Y-LRRK2
p.N1506Y-R	ATTAAGGCTCTCGTAT <u><b>A</b></u> TGATGGTTTTCCG	
p.I835L-F	AAGGAAACAAACAAATT <u><b>T</b></u> AGCATCTACACTAG	Mutant I835L-LRRK2
p.I835L-R	CTAGTGATAGTCT <u><b>A</b></u> AATTTGTTTGTTCCTT	
<b>For lentivirus construct <sup>b</sup></b>		
NotI-PLVX-F	ATAAGAAT <u><b>GCGGCCGC</b></u> ATGGCATCAATGCAGAAG	Forward primer for vector construction
MluI-PLVX-R	CG <u><b>ACGCGT</b></u> TTACTCAACAGATGTTTCGTCTC	Reverse primer for vector construction

<sup>a</sup> Restriction recognition sites are indicated with italic, bold and underlining fonts directed mutagenesis sites are highlighted in red. F-forward primer; R-reverse primer. <sup>b</sup> Primers used in our previous study [38].

## Supplementary References

1. Kilkenny, C, Browne, WJ, Cuthill, IC, *et al.* Improving bioscience research reporting: the ARRIVE guidelines for reporting animal research. *PLoS Biol.* 2010; **8**(6): e1000412.
2. Smith, RD, Zhang, Z, Kurlan, R, *et al.* Developing a stable bilateral model of parkinsonism in rhesus monkeys. *Neuroscience.* 1993; **52**(1): 7-16.
3. Imbert, C, Bezard, E, Guiraud, S, *et al.* Comparison of eight clinical rating scales used for the assessment of MPTP-induced parkinsonism in the Macaque monkey. *J Neurosci Methods.* 2000; **96**(1): 71-6.
4. Lei, X, Li, H, Huang, B, *et al.* 1-methyl-4-phenylpyridinium stereotactic infusion completely and specifically ablated the nigrostriatal dopaminergic pathway in rhesus macaque. *PLoS One.* 2015; **10**(5): e0127953.
5. Li, H, Lei, X, Huang, B, *et al.* A quantitative approach to developing Parkinsonian monkeys (*Macaca fascicularis*) with intracerebroventricular 1-methyl-4-phenylpyridinium injections. *J Neurosci Methods.* 2015; **251**: 99-107.
6. Bezard, E, Przedborski, S. A tale on animal models of Parkinson's disease. *Mov Disord.* 2011; **26**(6): 993-1002.
7. Beal, MF. Experimental models of Parkinson's disease. *Nature reviews Neuroscience.* 2001; **2**(5): 325-34.
8. Emborg, ME. Nonhuman primate models of Parkinson's disease. *ILAR J.* 2007; **48**(4): 339-55.
9. Dickson, DW, Braak, H, Duda, JE, *et al.* Neuropathological assessment of Parkinson's disease: refining the diagnostic criteria. *Lancet Neurol.* 2009; **8**(12): 1150-7.
10. Chu, Y, Kompoliti, K, Cochran, EJ, *et al.* Age-related decreases in Nurr1 immunoreactivity in the human substantia nigra. *J Comp Neurol.* 2002; **450**(3): 203-14.
11. Chu, Y, Kordower, JH. Age-associated increases of alpha-synuclein in monkeys and humans are associated with nigrostriatal dopamine depletion: Is this the target for Parkinson's disease? *Neurobiol Dis.* 2007; **25**(1): 134-49.
12. Chu, Y, Muller, S, Tavares, A, *et al.* Intra-striatal alpha-synuclein fibrils in monkeys: spreading, imaging and neuropathological changes. *Brain.* 2019.
13. Gundersen, HJ, Bagger, P, Bendtsen, TF, *et al.* The new stereological tools: disector, fractionator, nucleator and point sampled intercepts and their use in pathological research and diagnosis. *APMIS.* 1988; **96**(10): 857-81.
14. Huang, B, Wu, S, Wang, Z, *et al.* Phosphorylated alpha-Synuclein Accumulations and Lewy Body-like Pathology Distributed in Parkinson's Disease-Related Brain Areas of Aged Rhesus Monkeys Treated with MPTP. *Neuroscience.* 2018; **379**: 302-15.
15. Neumann, M, Kahle, PJ, Giasson, BI, *et al.* Misfolded proteinase K-resistant hyperphosphorylated alpha-synuclein in aged transgenic mice with locomotor deterioration and in human alpha-synucleinopathies. *J Clin Invest.* 2002; **110**(10): 1429-39.
16. Shahmoradian, SH, Lewis, AJ, Genoud, C, *et al.* Lewy pathology in Parkinson's disease consists of crowded organelles and lipid membranes. *Nat Neurosci.* 2019; **22**(7): 1099-109.
17. Bae, EJ, Yang, NY, Song, M, *et al.* Glucocerebrosidase depletion enhances cell-to-cell transmission of alpha-synuclein. *Nat Commun.* 2014; **5**: 4755.
18. Gan, L, Vargas, MR, Johnson, DA, *et al.* Astrocyte-specific overexpression of Nrf2 delays motor pathology and synuclein aggregation throughout the CNS in the alpha-synuclein mutant (A53T) mouse model. *J Neurosci.* 2012; **32**(49): 17775-87.
19. Kiely, AP, Asi, YT, Kara, E, *et al.* alpha-Synucleinopathy associated with G51D SNCA mutation: a link between Parkinson's disease and multiple system atrophy? *Acta Neuropathol.* 2013; **125**(5): 753-69.
20. Ling, H, Kara, E, Bandopadhyay, R, *et al.* TDP-43 pathology in a patient carrying G2019S LRRK2 mutation and a novel p.Q124E MAPT. *Neurobiol Aging.* 2013; **34**(12): 2889 e5-9.
21. Mestre-Frances, N, Serratrice, N, Gennetier, A, *et al.* Exogenous LRRK2G2019S induces parkinsonian-like pathology in a nonhuman primate. *JCI Insight.* 2018; **3**(14).
22. Lohmann, S, Bernis, ME, Tachu, BJ, *et al.* Oral and intravenous transmission of alpha-synuclein fibrils to mice. *Acta Neuropathol.* 2019; **138**(4): 515-33.
23. Garcia-Dominguez, I, Vesela, K, Garcia-Revilla, J, *et al.* Peripheral Inflammation Enhances Microglia Response and Nigral Dopaminergic Cell Death in an in vivo MPTP Model of Parkinson's Disease. *Front Cell Neurosci.* 2018; **12**: 398.
24. Kimura, K, Inoue, KI, Kuroiwa, Y, *et al.* Propagated but Topologically Distributed Forebrain Neurons Expressing Alpha-Synuclein in Aged Macaques. *PLoS One.* 2016; **11**(11): e0166861.
25. Wegrzynowicz, M, Bar-On, D, Calo, L, *et al.* Depopulation of dense alpha-synuclein aggregates is associated with rescue of dopamine neuron dysfunction and death in a new Parkinson's disease model. *Acta Neuropathol.* 2019; **138**(4): 575-95.

26. Poewe, W, Seppi, K, Tanner, CM, *et al.* Parkinson disease. *Nat Rev Dis Primers*. 2017; **3**: 17013.
27. Kraemmer, J, Kovacs, GG, Perju-Dumbrava, L, *et al.* Correlation of striatal dopamine transporter imaging with post mortem substantia nigra cell counts. *Mov Disord*. 2014; **29**(14): 1767-73.
28. Houlden, H, Singleton, AB. The genetics and neuropathology of Parkinson's disease. *Acta Neuropathol*. 2012; **124**(3): 325-38.
29. Singleton, AB, Farrer, MJ, Bonifati, V. The genetics of Parkinson's disease: progress and therapeutic implications. *Mov Disord*. 2013; **28**(1): 14-23.
30. Boyle, EA, O'Roak, BJ, Martin, BK, *et al.* MIPgen: optimized modeling and design of molecular inversion probes for targeted resequencing. *Bioinformatics*. 2014; **30**(18): 2670-2.
31. Hardenbol, P, Baner, J, Jain, M, *et al.* Multiplexed genotyping with sequence-tagged molecular inversion probes. *Nat Biotechnol*. 2003; **21**(6): 673-8.
32. Nilsson, M, Malmgren, H, Samiotaki, M, *et al.* Padlock probes: circularizing oligonucleotides for localized DNA detection. *Science*. 1994; **265**(5181): 2085-8.
33. O'Roak, BJ, Vives, L, Fu, W, *et al.* Multiplex targeted sequencing identifies recurrently mutated genes in autism spectrum disorders. *Science*. 2012; **338**(6114): 1619-22.
34. Wang, T, Guo, H, Xiong, B, *et al.* De novo genic mutations among a Chinese autism spectrum disorder cohort. *Nat Commun*. 2016; **7**: 13316.
35. Li, H, Durbin, R. Fast and accurate long-read alignment with Burrows-Wheeler transform. *Bioinformatics*. 2010; **26**(5): 589-95.
36. Kircher, M, Witten, DM, Jain, P, *et al.* A general framework for estimating the relative pathogenicity of human genetic variants. *Nat Genet*. 2014; **46**(3): 310-5.
37. Rentzsch, P, Witten, D, Cooper, GM, *et al.* CADD: predicting the deleteriousness of variants throughout the human genome. *Nucleic Acids Res*. 2019; **47**(D1): D886-D94.
38. Wang, D, Xu, L, Lv, L, *et al.* Association of the LRRK2 genetic polymorphisms with leprosy in Han Chinese from Southwest China. *Genes Immun*. 2015; **16**(2): 112-9.
39. Su, LY, Li, H, Lv, L, *et al.* Melatonin attenuates MPTP-induced neurotoxicity via preventing CDK5-mediated autophagy and SNCA/alpha-synuclein aggregation. *Autophagy*. 2015; **11**(10): 1745-59.
40. Su, LY, Luo, R, Liu, Q, *et al.* Atg5- and Atg7-dependent autophagy in dopaminergic neurons regulates cellular and behavioral responses to morphine. *Autophagy*. 2017; **13**(9): 1496-511.
41. Xu, M, Zhang, DF, Luo, R, *et al.* A systematic integrated analysis of brain expression profiles reveals YAP1 and other prioritized hub genes as important upstream regulators in Alzheimer's disease. *Alzheimers Dement*. 2018; **14**(2): 215-29.
42. Kim, D, Langmead, B, Salzberg, SL. HISAT: a fast spliced aligner with low memory requirements. *Nat Methods*. 2015; **12**(4): 357-60.
43. Liao, Y, Smyth, GK, Shi, W. featureCounts: an efficient general purpose program for assigning sequence reads to genomic features. *Bioinformatics*. 2014; **30**(7): 923-30.
44. Love, MI, Huber, W, Anders, S. Moderated estimation of fold change and dispersion for RNA-seq data with DESeq2. *Genome Biol*. 2014; **15**(12): 550.
45. Huang da, W, Sherman, BT, Lempicki, RA. Systematic and integrative analysis of large gene lists using DAVID bioinformatics resources. *Nat Protoc*. 2009; **4**(1): 44-57.
46. Kalia, LV, Lang, AE. Parkinson's disease. *Lancet*. 2015; **386**(9996): 896-912.
47. Lees, AJ, Hardy, J, Revesz, T. Parkinson's disease. *Lancet*. 2009; **373**(9680): 2055-66.
48. Roth, GS, Mattison, JA, Ottinger, MA, *et al.* Aging in rhesus monkeys: relevance to human health interventions. *Science*. 2004; **305**(5689): 1423-6.
49. Tigges, J, Gordon, TP, McClure, HM, *et al.* Survival rate and life span of rhesus monkeys at the Yerkes regional primate research center. *Am J Primatol*. 1988; **15**(3): 263-73.
50. Yu, L, Gaitatzes, C, Neer, E, *et al.* Thirty-plus functional families from a single motif. *Protein Sci*. 2000; **9**(12): 2470-6.
51. Mata, IF, Wedemeyer, WJ, Farrer, MJ, *et al.* LRRK2 in Parkinson's disease: protein domains and functional insights. *Trends Neurosci*. 2006; **29**(5): 286-93.
52. Ramirez, A, Heimbach, A, Grundemann, J, *et al.* Hereditary parkinsonism with dementia is caused by mutations in ATP13A2, encoding a lysosomal type 5 P-type ATPase. *Nat Genet*. 2006; **38**(10): 1184-91.
53. Yang, X, Xu, Y. Mutations in the ATP13A2 gene and Parkinsonism: a preliminary review. *Biomed Res Int*. 2014; **2014**: 371256.
54. Cookson, MR. The role of leucine-rich repeat kinase 2 (LRRK2) in Parkinson's disease. *Nature reviews Neuroscience*. 2010; **11**(12): 791-7.
55. Xu, Q, Guo, H, Zhang, X, *et al.* Hypoxia regulation of ATP13A2 (PARK9) gene transcription. *J Neurochem*. 2012; **122**(2): 251-9.
56. Eysers, PA. Back to the future: new target-validated Rab antibodies for evaluating LRRK2 signalling in cell biology and Parkinson's disease. *Biochem J*. 2018; **475**(1): 185-9.